Annales Geophysicae (2002) 20: 1447–1467 © European Geophysical Society 2002

Annales Geophysicae

Temperature tides determined with meteor radar

W. K. Hocking[1] **and A. Hocking**[2]

[1]Dept. of Physics and Astronomy, University of Western Ontario, London, Ont., N6A 3K7, Canada
[2]Mardoc Inc., London, Ont., N6G 4N4, Canada

Received: 12 November 2001 – Revised: 30 April 2002 – Accepted: 19 June 2002

Abstract. A new analysis method for producing tidal temperature parameters using meteor radar measurements is presented, and is demonstrated with data from one polar and two mid-latitude sites. The technique further develops the temperature algorithm originally introduced by Hocking (1999). That earlier method was used to produce temperature measurements over time scales of days and months, but required an empirical model for the mean temperature gradient in the mesopause region. However, when tides are present, this temperature gradient is modulated by the presence of the tides, complicating extraction of diurnal variations. Nevertheless, if the vertical wavelengths of the tides are known from wind measurements, the effects of the gradient variations can be compensated for, permitting determination of temperature tidal amplitudes and phases by meteor techniques. The basic theory is described, and results from meteor radars at Resolute Bay (Canada), London (Canada) and Albuquerque (New Mexico, USA) are shown. Our results are compared with other lidar data, computer models, fundamental tidal theory and rocket data. Phase measurements at two mid-latitude sites (Albuquerque, New Mexico, and London, Canada) show times of maximum for the diurnal temperature tide to change modestly throughout most of the year, varying generally between 0 h and 6 h, with an excursion to 12 h in June at London. The semidiurnal tide shows a larger annual variation in time of maximum, being at 2–4 h in the winter months but increasing to 9 h during the late summer and early fall. We also find that, at least at mid-latitudes, the phase of the temperature tide matches closely the phase of the meridional tide, and theoretical justification for this statement is given. We also demonstrate that this is true using the Global Scale Wave Model (Hagan et al., 1999). Median values for the temperature amplitudes for each site are in the range 5 to 6 Kelvin. Results from a more northern site (Resolute Bay) show less consistency between the wind tides and the temperature tides, supporting suggestions that the temperature tides may be zonally symmetric at these high latitudes (e.g. Walterscheid and Sivjee, 2001).

Key words. Meteorology and atmospheric dynamics (middle atmosphere dynamics; waves and tides) – Radio science (signal processing)

Correspondence to: A. Hocking (mardoc-inc@rogers.com)

1 Introduction

Recent papers (Hocking et al., 1997; Hocking 1999) have demonstrated how meteor radars can be utilized to measure temperatures around the mesopause region. One method (Hocking et al., 1997) requires knowledge of the pressure at the height of radio scatter, and is not recommended, since the CIRA pressures are too unreliable for useful application. This method does, however, permit a height profile of temperatures to be determined if (and only if) the pressures can be properly measured. The method is probably more useful when it is combined with temperature data from other instruments to allow for the determination of atmospheric pressures in the meteor region.

The second method (Hocking, 1999) produces only a height-averaged temperature in the meteor region, but requires no a-priori knowledge of atmospheric pressure. For best results, however, some approximation to the mean temperature gradient is required, and this is usually provided by an empirical model. A suitable expression was given in Hocking (1999), but subsequent studies with lidar observations at various sites have led to some refinements, notably in the polar regions. Complications also occur in the polar summer region because the mesopause can alternate between a height above the meteor peak and a height below this peak. We will not discuss the newer empirical temperature-gradient in this paper because is not critical to the determination of tidal amplitudes, which are our main focus in this paper.

Generally, several hundred meteor detections are required, in order to make a successful temperature measurement, and several thousand meteors are preferred. Hence, meteor radars generally produce temperatures which are daily averages, or

even 2 or 3 day averages. The fact that the averaging period is so long permits us to use moderately slowly varying model seasonal values for the temperature gradient.

However, it is also desirable to extract tidal information in relation to temperature. In principle, this can be done using "superposed epoch analyses" (also called "composite day" analyses), in which meteors are binned into hourly (or 2-hourly) bins as a function of time of day, using data from extended time periods (typically 10 days to one month). This allows us to achieve the desired count rates of several thousand meteors per bin. We may then use the standard temperature-determination algorithm (Hocking, 1999) to determine the temperature in each bin, providing that the temperature gradient is known. This gives us, therefore, a "typical" diurnal variation, at least to the first order.

In this paper, we assume that most of the diurnal variation of the temperatures is due to atmospheric tides. If the tides are of short vertical wavelength (e.g. $\leq$ 40 km), then the temperature gradient itself shows a diurnal variation, and a proper determination of the diurnal variation in temperature should consider this fact. If the vertical wavelength is known, for example, from determination of meteor winds, then it is possible to compensate for these variations in gradient. Indeed, the temperature amplitudes for the diurnal and semidiurnal tide deduced by this process are not only robust, but are also largely independent of the assumed value for the mean daily (seasonal) temperature gradient.

In this paper, we describe the theory behind the determination of temperature tides by this procedure. Results are compared with values achieved if the diurnal variation in temperature gradient is not considered. We find that proper consideration of the gradient in this way typically produces amplitudes of the order of 20% less than those obtained with the more naive procedures, and can alter the phase by up to 2 h.

Section 2 outlines the basic theory used in our considerations. We permit arbitrary diurnal and semidiurnal tides, but not terdiurnal tides, in our initial theory. In Sect. 3 we show results of our procedures from various sites using SKiYMET radars (Hocking et al., 2001), and present annual variations in tidal amplitude and phase for both diurnal and semidiurnal components for sites near London (Ontario, Canada), Albuquerque (New Mexico, USA) and Resolute Bay (Nunavut, Canada). We also compare our results to published tidal amplitudes and phases deduced by lidar techniques (States and Gardner, 2000a, b). Similar lidar measurements have been presented by Chen et al. (2000), but we will concentrate our comparisons on the data of States and Gardner (2000a). Our temperature tidal amplitudes often appear substantially larger than modeling suggests should occur, so in Sect. 4 we present data from earlier meteorological rocket studies which show that amplitudes of the order of those that we measure are reasonable. We also find a frequent close similarity between the phases of the temperature tide and the meridional wind, and in Sect. 5 we present the theoretical background as to why this is true. In Sect. 6 we discuss our results in a general context, and in Sect. 7 we present our conclusions.

2 Basic theory

As a starting point to our analysis, we assume that we have recorded temperatures as a function of hour of day via a superposed epoch analysis, and have fitted diurnal, semidiurnal, and terdiurnal components. Figure 1a shows an example of such a fitting process.

We will assume that each temperature was determined (following Hocking, 1999) using an assumed (fixed) temperature gradient $\left(\frac{dT}{dz}\right)_0$. It will in fact turn out that our final tidal temperature amplitudes will be largely independent of our choice of $\left(\frac{dT}{dz}\right)_0$, but for now we will let this parameter be general in value.

The value of the temperature in each bin derived using this (fixed) value for $\left(\frac{dT}{dz}\right)_0$ will be denoted as $T_{naive}(i)$, where i is the bin number. Then, following (Hocking, 1999),

$$T_{naive} = S_m \log_e \left(\frac{Mg}{R} + 2\left(\frac{dT}{dz}\right)_0 \right), \tag{1}$$

where M is the molar mass of the atmosphere, g is the acceleration due to gravity, and R is the ideal gas constant.

A more accurate value for the temperature would, however, be

$$T_{true} = S_m \log_e \left(\frac{Mg}{R} + 2\left(\frac{dT}{dz}\right)_t \right), \tag{2}$$

where $\left(\frac{dT}{dz}\right)_t$ is the true (unknown) temperature gradient at the time of measurement. This parameter will in fact vary as a function of time of day, as the tide changes.

By comparing the two previous equations, we see that we may write that

$$T_{true} = T_{naive} \left[\frac{\frac{Mg}{R} + 2\left(\frac{dT}{dz}\right)_t}{\frac{Mg}{R} + 2\left(\frac{dT}{dz}\right)_0} \right]. \tag{3}$$

We will write this as

$$T_{true} = T_{naive} B \left[1 + A\left(\frac{dT}{dz}\right)_t \right], \tag{4}$$

where $B = \left(\frac{Mg}{R}\right) / \left[\frac{Mg}{R} + 2\left(\frac{dT}{dz}\right)_0\right]$ and $A = \frac{2R}{Mg}$.

We now assume that the temporal variation of T_{naive} can be written as the sum of harmonic components, viz

$$\begin{aligned} T_{naive} = {} & T_{0N} + F_D \in_{DN} \cos\left(\frac{2\pi}{\tau_D}t + \phi_{DN}\right) \\ & + F_S \in_{SN} \cos\left(\frac{2\pi}{\tau_S}t + \phi_{SN}\right) \\ & + F_T \in_{TN} \cos\left(\frac{2\pi}{\tau_T}t + \phi_{TN}\right). \end{aligned} \tag{5}$$

Here, the subscript "N" in the various terms reminds us that this is a fit to the "naive" hourly temperature data. T_{0N} is

the mean value of T_{naive}, $\in_{DN}$ is the amplitude of the (naive) fitted diurnal component, ϕ_{DN} is the phase of the fitted diurnal component, $\in_{SN}$ is the amplitude of the fitted semidiurnal component, ϕ_{SN} is the phase of the fitted semidiurnal component, $\in_{TN}$ is the amplitude of the fitted terdiurnal component, ϕ_{TN} is the phase of the fitted terdiurnal component. The quantities τ_D, τ_S and τ_T represent the periods of the three major harmonics (24 h, 12 h, and 8 h, respectively). Fourth and higher harmonics could be included, but for now we assume that they are small in amplitude.

We also need to describe the meaning of the terms F_D, F_S and F_T in the previous expression. These represent spatial filters, and require some explanation, which is now given.

The effective temperatures which we determine are actually an average in height. If we have a single tidal component, then in any time bin we measure a quantity

$$T = \int W(z) T_0 \cos(mz + \phi) dz, \tag{6}$$

where m is the vertical wave number of the tidal component and $W(z)$ is a weighting function which follows the meteor count-rate profile. Thus, the temperature that we measure is a weighted average across the depth of the "meteor region". Tides with very short vertical wavelengths will have substantially suppressed measured tidal amplitudes, and tides with very long vertical wavelengths (much longer than the depth of the meteor layer) will suffer almost no suppression. The quantities F_D, F_S and F_T represent filter functions that describe the level of suppression, and they may take values between 0 and 1. They are particularly dependent on the ratio between the depth of the meteor layer and the vertical wavelength of the tide.

We now assume that the true temperature variation as a function of time can be represented by

$$\begin{aligned} T_{true} = T_{0t} &+ F_D \in_{Dt} \cos\left(\frac{2\pi}{\tau_D} t + \phi_{Dt}\right) \\ &+ F_S \in_{St} \cos\left(\frac{2\pi}{\tau_S} t + \phi_{St}\right), \end{aligned} \tag{7}$$

where the subscript "t" means "true" temperatures. Notice we have assumed only diurnal and semidiurnal components in this case, for reasons to be described shortly.

Then, the temperature gradient in each time bin varies, and is given by

$$\begin{aligned} \left(\frac{dT}{dz}\right)_{true} = &\left(\frac{dT}{dz}\right)_{0t} \\ &- F_D m_D \in_{Dt} \sin\left(\frac{2\pi t}{\tau_D} + \phi_{Dt}\right) \\ &- F_S m_S \in_{St} \sin\left(\frac{2\pi t}{\tau_S} + \phi_{St}\right), \end{aligned} \tag{8}$$

where m_D and m_S are the vertical wave numbers of the diurnal and semidiurnal tides, respectively. Note that this is a time-varying quantity, so both the absolute temperature and the gradient vary with time. We wish to utilize our measured "naive" tidal amplitudes and phases ($\in_{DN}$, ϕ_{DN}, $\in_{SN}$, ϕ_{SN}, $\in_{TN}$ and ϕ_{TN}) to derive the true values ($\in_{Dt}$, ϕ_{Dt}, $\in_{St}$ and ϕ_{St}).

From Eq. (4), and recognizing that the term $A\left(\frac{dT}{dz}\right)_t$ is generally much less than unity, we may write

$$T_{naive} = \frac{T_{true}}{B} - \frac{A}{B} T_{true} \left(\frac{dT}{dz}\right)_{true}. \tag{9}$$

It can be seen that T_{naive} involves a term which is a product of the true temperature and the temperature gradient, both of which contain various harmonics. Hence, T_{naive} will involve even higher harmonics – for example, if T_{true} contains first, second and third harmonics (diurnal, semidiurnal and terdiurnal components), then T_{naive} may contain up to the sixth harmonic. This is why at present we only permit T_{true} to obtain diurnal and semidiurnal components; it restricts T_{naive} to contain only quardiurnal components at maximum. Later, we will fit a linear combination of first, second and third harmonics to our T_{naive} values, in order to determine diurnal and semidiurnal components in T_{true}. If we wanted to retrieve a terdiurnal component in T_{true}, we would need to fit T_{naive} to the sixth harmonic, and past experience has shown that the errors on the fifth and sixth harmonics can be very large, and the values unreliable. Hence, we restrict ourselves to cases where the terdiurnal component is known to be weak (as determined from wind tidal measurements), and concentrate on diurnal and semidiurnal temperature tides for now. Further advances on this theory to include higher harmonics may be included at a later time once some level of confidence is established in the current procedures.

Expanding each side of Eq. (9) in terms of harmonic components, as shown in Eqs. (5), (7) and (8), gives

$$\begin{aligned} &T_{0N} + F_{DN} \in_{DN} \cos\left(\frac{2\pi t}{\tau_D} + \phi_{DN}\right) \\ &\quad + F_{SN} \in_{SN} \cos\left(\frac{2\pi t}{\tau_S} + \phi_{SN}\right) \\ &\quad + F_{TN} \in_{TN} \cos\left(\frac{2\pi t}{\tau_T} + \phi_{TN}\right) \\ &\quad = \frac{T_{0t}}{B} + \frac{F_{Dt}}{B} \in_{Dt} \cos\left(\frac{2\pi t}{\tau_D} + \phi_{Dt}\right) \\ &\quad + \frac{F_{St}}{B} \in_{St} \cos\left(\frac{2\pi t}{\tau_S} + \phi_{St}\right) \\ &\quad - \frac{A}{B}\left[T_{0t} + F_{Dt} \in_{Dt} \cos\left(\frac{2\pi t}{\tau_D} + \phi_{Dt}\right)\right. \\ &\quad \left. + F_{St} \in_{St} \cos\left(\frac{2\pi t}{\tau_S} + \phi_{St}\right)\right] \\ &\quad \times\left[\left(\frac{dT}{dz}\right)_{0t} - F_{Dt} m_D \in_{Dt} \sin\left(\frac{2\pi t}{\tau_D} + \phi_{Dt}\right)\right. \\ &\quad \left. - F_{St} m_S \in_{St} \sin\left(\frac{2\pi t}{\tau_S} + \phi_{St}\right)\right]. \end{aligned} \tag{10}$$

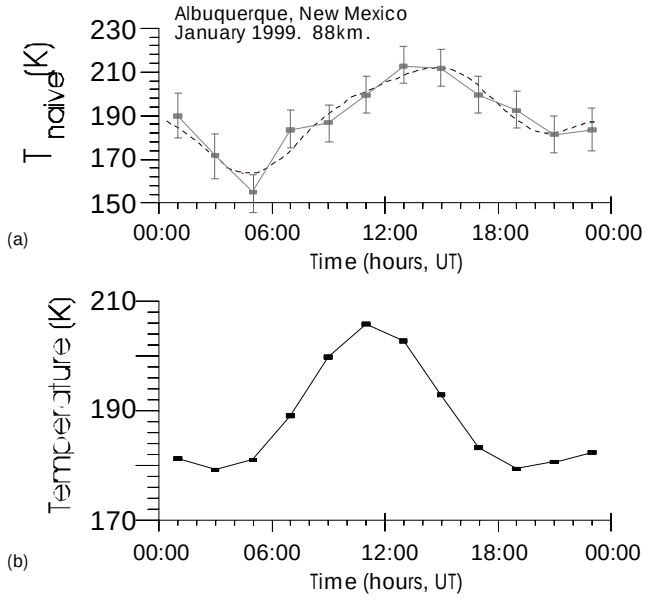

Fig. 1. (a) Graph showing the mean "naive" temperature as a function of time of day for a composite day for January 1999 over Albuquerque, New Mexico. A best fit diurnal plus semidiurnal plus terdiurnal curve is also shown. **(b)** "True" temperature versus time of day after compensation for the introduction of artificial higher order modes that arise as a result of effects associated with the daily variation of the temperature gradient in the extraction of meteor-derived temperatures.

The filter functions can readily be evaluated for any prespecified vertical wavelength by evaluating Eq. (6). We actually perform the determination in the Fourier domain, which makes it much faster. Since the phase term ϕ is not known, we normally average over several phases to produce a typical "average" filter. We also assume that $F_{DN} = F_{Dt} = F_D$, and $F_{SN} = F_{St} = F_S$. If the vertical wavelength is known, the above equation can be solved uniquely for the five unknowns, T_{0t}, $\in_{Dt}$, ϕ_{Dt}, $\in_{St}$ and ϕ_{St}. A detailed solution of these equations involves expansion into mean, cosine and sine terms, and equating like harmonics.

Ideally, we would like to solve these equations exactly, but an analytical solution involves an enormous number of terms. Therefore, we settle for solving (initially) just for the diurnal and semidiurnal components, and assume for now that other terms are small. However, this will not be our final solution, but simply a starting point for a better solution, so we will eventually make use of even the terdiurnal components of the T_{naive} fit. Even when we just concentrate on the diurnal and semidiurnal terms, almost 50 individual terms are involved, but after some manipulation the following simpler equations emerge:

$$T_{0N} = \frac{T_{0t}}{B} - \frac{A}{B} T_{0t} \left(\frac{dT}{dz}\right)_{0t} \tag{11}$$

$$\begin{aligned}\in_{DN} \cos(\phi_{DN}) = {} & \frac{1}{B} \in_{Dt} \cos(\phi_{Dt}) \\ & + \frac{A}{B} T_{0t} m_D \in_{Dt} \sin(\phi_{Dt}) \\ & - \frac{A}{B} \left(\frac{dT}{dz}\right)_{0t} \in_{Dt} \cos(\phi_{Dt}) \\ & + \frac{1}{2} \frac{A}{B} F_S \in_{Dt} \in_{St} m_S \sin(\phi_{St} - \phi_{Dt}) \\ & - \frac{1}{2} \frac{A}{B} F_S \in_{St} \in_{Dt} m_D \sin(\phi_{St} - \phi_{Dt})\end{aligned} \tag{12}$$

$$\begin{aligned}\in_{DN} \sin(\phi_{DN}) = {} & \frac{1}{B} \in_{Dt} \sin(\phi_{Dt}) \\ & - \frac{A}{B} T_{0t} m_D \in_{Dt} \cos(\phi_{Dt}) \\ & - \frac{A}{B} \left(\frac{dT}{dz}\right)_{0t} \in_{Dt} \sin(\phi_{Dt}) \\ & - \frac{1}{2} \frac{A}{B} F_S \in_{Dt} \in_{St} m_S \cos(\phi_{St} - \phi_{Dt}) \\ & + \frac{1}{2} \frac{A}{B} F_S \in_{St} \in_{Dt} m_D \cos(\phi_{St} - \phi_{Dt})\end{aligned} \tag{13}$$

$$\begin{aligned}\in_{SN} \cos(\phi_{SN}) = {} & \frac{1}{B} \in_{St} \cos(\phi_{St}) \\ & + \frac{A}{B} T_{0t} m_S \in_{St} \sin(\phi_{St}) \\ & - \frac{A}{B} \left(\frac{dT}{dz}\right)_{0t} \in_{St} \cos(\phi_{St}) \\ & + \frac{A}{B} \frac{F_D^2}{F_S} \in_{Dt}^2 m_D \sin(\phi_{Dt}) \cos(\phi_{Dt})\end{aligned} \tag{14}$$

$$\begin{aligned}\in_{SN} \sin(\phi_{SN}) = {} & \frac{1}{B} \in_{St} \sin(\phi_{St}) \\ & - \frac{A}{B} T_{0t} m_S \in_{St} \cos(\phi_{St}) \\ & - \frac{A}{B} \left(\frac{dT}{dz}\right)_{0t} \in_{St} \sin(\phi_{St}) \\ & - \frac{1}{2} \frac{A}{B} \frac{F_D^2}{F_S} \in_{Dt}^2 m_D \left(2\cos^2(\phi_{Dt}) - 1\right),\end{aligned} \tag{15}$$

where $\left(\frac{dT}{dz}\right)_{0t}$ represents the average true temperature gradient for the whole day. The tidal components are only weakly dependent on this term, and use of an empirical model is sufficient. Indeed errors in this assumed slope affect primarily the calculated daily mean temperature, and have little impact on the tidal amplitudes and phases.

The vertical wavelength (where available) can be found from the wind components determined by the meteor radar by fitting temporal diurnal, semidiurnal and terdiurnal harmonic components to the wind components in the usual way.

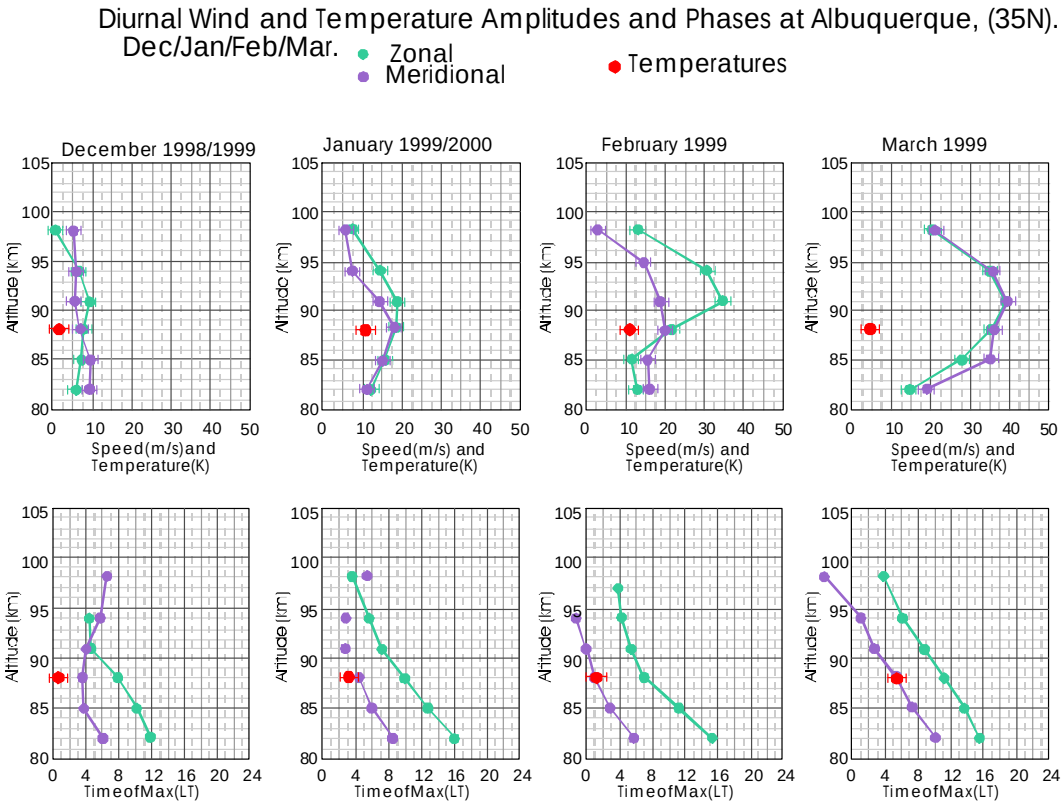

Fig. 2. Graphs showing examples of the diurnal tidal parameters deduced using the meteor radar at Albuquerque, New Mexico (35° N). Shown are height profiles of amplitudes and phases for the winds, as well as estimates of the temperature amplitudes and phases at 88 km altitude. The values are seasonal vector averages over several years, as indicated in the table at the base of the figure. Error bars are shown for the amplitudes and the temperature phase. No error bars are shown for the wind phases, since they are less than the sizes of the symbols used.

Cases where the terdiurnal wind component is large are excluded from further analysis. Thus, the meteor radar provides all the information needed to apply the method.

It should be noted that even though we assume only mean, diurnal and semidiurnal components in the "true" temporal variation of T, the "naive" temperature variations will contain artificial terdiurnal and higher components due to the cross terms involved in Eq. (10). Thus, the values for $\in_{TN}$ and ϕ_{TN} are in fact combinations of $\in_{Dt}$, ϕ_{Dt}, $\in_{St}$ and ϕ_{St}, and do not represent true terdiurnal tidal oscillations.

Solution of Eqs. (12) to (15) is a relatively simple procedure, which will not be elaborated upon here, and we can readily produce values for $\in_{Dt}$, ϕ_{Dt}, $\in_{St}$ and ϕ_{St}. However, we have already indicated that this solution is not our final answer, but a starting point for a more exact solution. The previous solution essentially ignored the terdiurnal component in even the "naive" fit. We now wish to go beyond this assumption.

In order to do this, we adopt the following solution. The previous procedure involved a two-step process. First, we applied a least-squares harmonic fit to the T_{naive} values, and then we solved a separate set of Eqs. (12) to (15). This gave us a set of coefficients which can now serve as a starting point for the next step. We now perform a least-squares harmonic fit of the transformation function directly on the T_{naive} values. We do this by using a least-squares minimization search algorithm, as described below, using the values for $\in_{Dt}$, ϕ_{Dt}, $\in_{St}$ and ϕ_{St}, as determined above, as the starting points for our minimization.

This procedure is performed in the following way. Rather than fit harmonic components to the observations, we fit the more complicated function on the right-hand side of Eq. (10) directly to the raw data. Thus, if the raw data points are given by $R(t_i)$, and the function on the right-hand side of Eq. (10) is described by $L(t, T_{0t}, \in_{Dt}, \phi_{Dt}, \in_{St}, \phi_{St})$, then we simply minimize the quantity

$$\Lambda^2 = \Sigma_{i=1}^{24} \left[R(t_i) - L(t_i, T_{0t}, \in_{dt}, \in_{Dt}, \phi_{Dt}, \in_{St}, \phi_{St}) \right]^2, \qquad (16)$$

where t_i are the time bins, which here have been taken to occur at steps of 1 h. Notice we allow T_{0t} to be a free variable as well.

Minimization of this quantity as a function of the variables of L can easily be achieved using standard algorithms (e.g. Bevington, 1969). We use the values derived in the first procedure as starting points for our final determinations by the

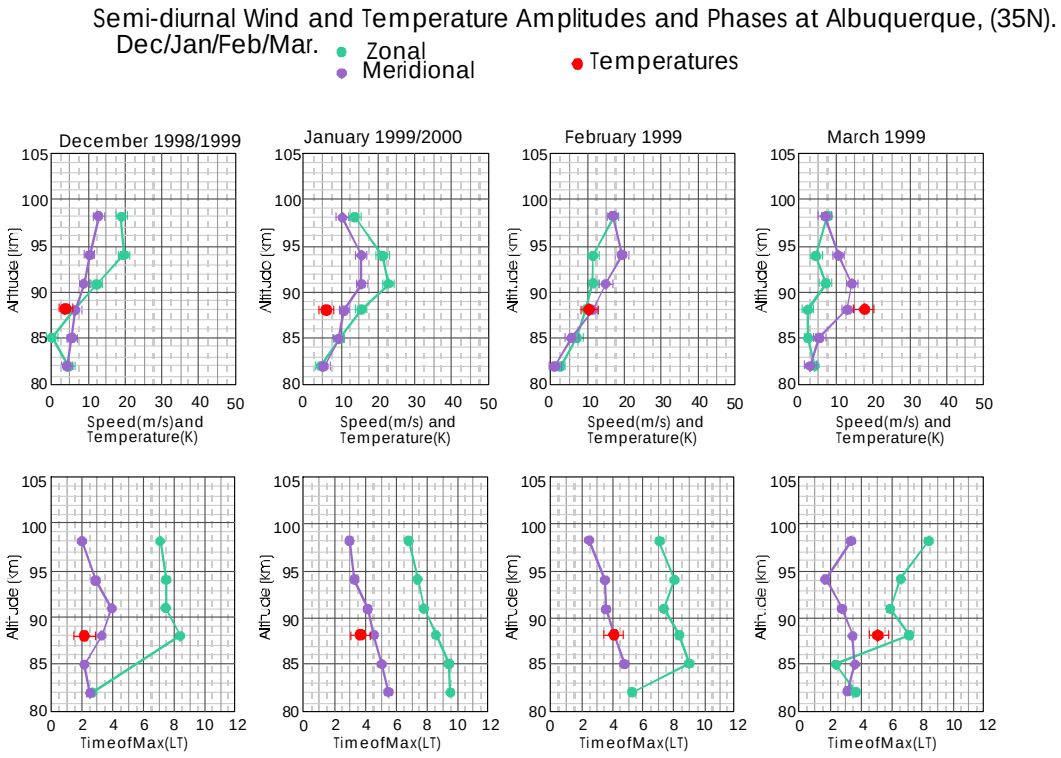

Fig. 3. As for Fig. 2, but for semidiurnal components at Albuquerque.

second procedure. Thus, determination of the terms can be achieved.

An example of the application of these procedures is shown in Fig. 1. Figure 1a shows the temporal variation of the "naive" temperature, and then Fig. 1b shows the variation of the "true" temperature. The vertical wavelengths have been determined from the wind tides, as described earlier. It is clearly seen that the "true" temporal variation differs from the "naive" values, both in phase and amplitude. The true temperatures show a smoother variation, which is to be expected, since some of the higher-order oscillations in the naive values are in fact due to mathematical coupling between the first and second harmonics. In cases where the vertical wavelength approaches infinity, the "naive" and "true" temporal variations become identical.

3 Results of application

In this section we present the results of the application of this theory to data from sites at Resolute Bay (Nunavut, Canada), London (Ontario, Canada) and Albuquerque (New Mexico, USA). We compare results with two different references; first we compare them with the GSWM of Hagan et al. (1995, 1999), and second, with a detailed set of lidar observations at Illinois by States and Gardner (2000a, b). With regard to our observations at Resolute Bay, we make some general comparisons with various types of meteorological rocket data.

To begin, Fig. 2 shows meteor wind data recorded with the meteor radar located at Albuquerque, New Mexico. This radar operates according to the description in Hocking et al. (2001), and functions at a frequency of 35.24 MHz. Typical height profiles are shown for both the diurnal amplitudes and phases. Error estimates are shown, as based on the determinations of Thayaparan and Hocking (2002). These data are especially important for temperature determinations, because it is these data which enable us to determine the vertical wavelengths. For example, the March data show very well-defined phase progressions with height, from which the vertical wavelength of the diurnal tide can clearly be seen to be about 30 km. Determination of vertical wavelengths for the February and January data is also possible, though not as obviously as for March. The December data shows an example where determination of vertical wavelengths is harder to ascertain, although the meridional component seems to be evanescent and the zonal components have a vertical wavelength of the order of 30 km in the 82 to 92 km region. Cases in which the vertical wavelength cannot be properly determined are generally excluded from further temperature analysis, although in some cases we can place lower limits on the vertical wavelength, which can still be useful. In cases where the wavelength cannot be found easily, but is clearly quite long, we may also extract useful temperature tides, because in those cases the variation from the "naive" fit is not large. Figure 3 shows similar plots, but for the semidiurnal tides. The temperature tides are also shown, but we will return to a greater discussion about these shortly.

Figures 4 and 5 show some comparisons between various mid-latitude measurements of temperature tides in the

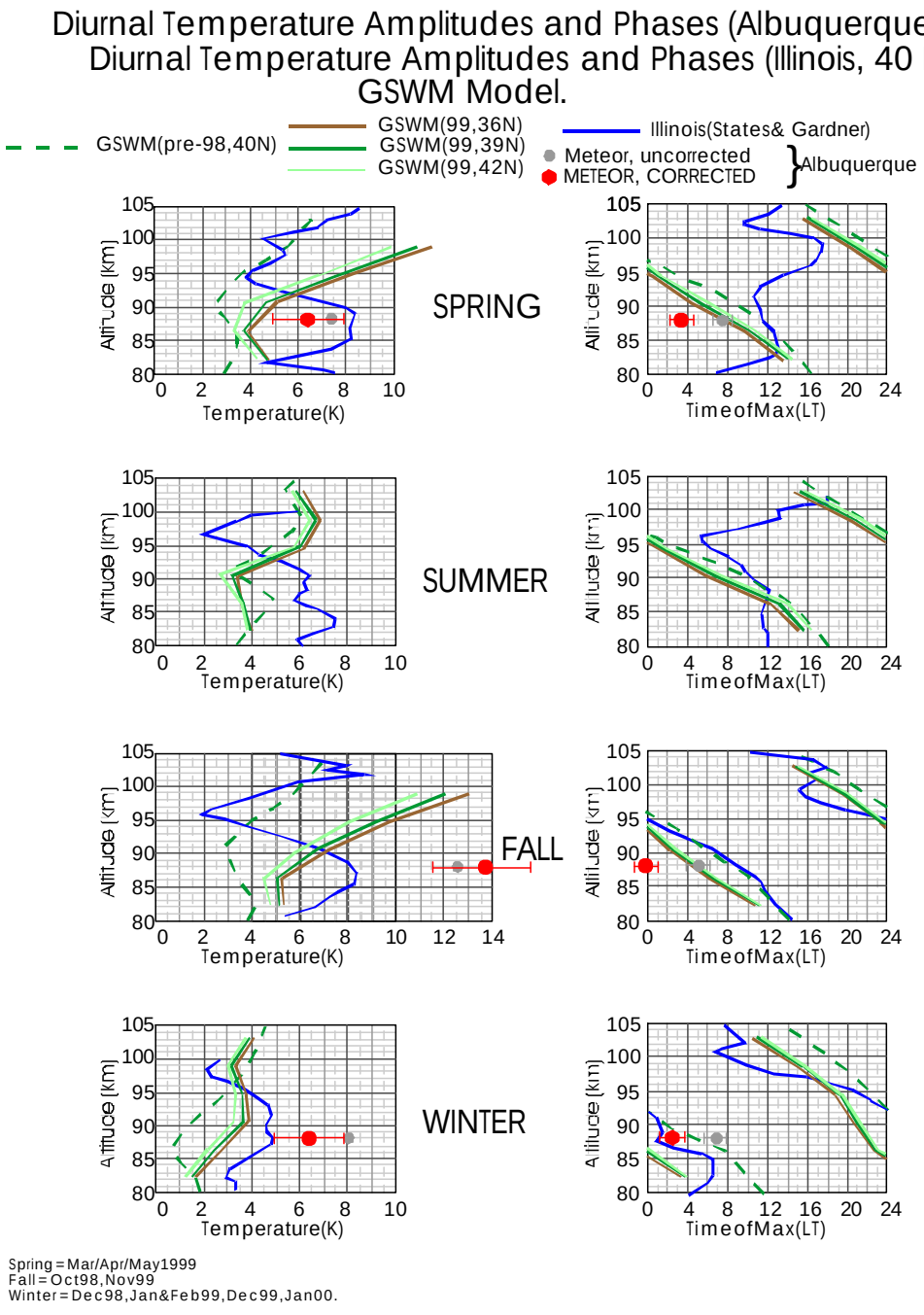

Fig. 4. Various estimates of the anticipated diurnal temperature tidal amplitudes and phases in the altitude band 35 to 42° N. Shown are estimates from the Global Scale Wave Model (Hagan et al., 1999), an earlier version of the GSWM, measurements due to States and Gardner (2000b), as well as two sets of estimates of diurnal temperature parameters made by meteor radar. The "uncorrected" meteor radar temperatures are also referred to as "naive" temperatures in the text, whereas the "corrected" temperatures are referred to as "true" temperatures in the text. Error bars are given for the "true" amplitudes, and for both true and naive phases. The error bars for the naive amplitudes are not given, but are the same as for the corresponding true amplitudes.

atmosphere, for diurnal and semidiurnal components, respectively. These include lidar measurements (States and Gardner, 2000a, b) made using a lidar capable of daytime temperature measurements, as well as results from a numerical model, and also results from the meteor radar at Albuquerque. The lidar data were acquired at Champaign-Urbana, Illinois, USA. The GSWM data (Hagan et al., 1995, 1999) were extracted for 3 latitudes from 36 to 42° N. Notice from the GSWM profiles that there is not a large variation in either the amplitude or phase between the two extremes of the latitudes shown, so it is reasonable to compare these data from different latitudes. The meteor data are shown

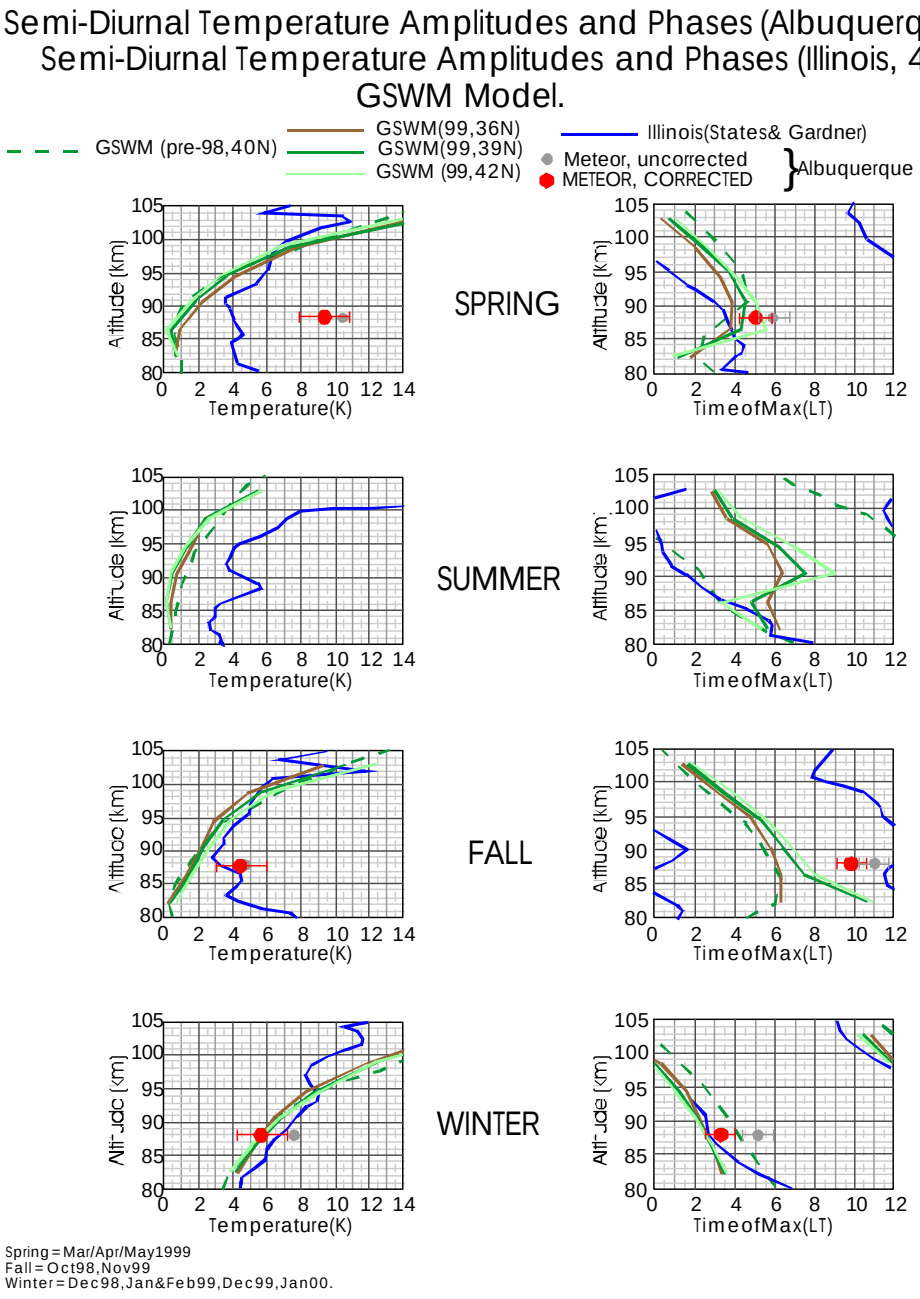

Fig. 5. As for Fig. 4, but for the semidiurnal temperature tide at Albuquerque.

for both the "naive" fits and the "true" fits as seasonal averages. Some temperature tidal parameters for the months of December, January, February and March are also shown in Figs. 2 and 3. It should be noted that the meteor site had large amounts of impulsive noise and interference, particularly due to discharges produced on nearby power lines, which often reduced our data quantities significantly. It was generally possible to deduce winds from the radar data, but the temperature analyses required much higher data rates, in order to achieve sufficient significance, and some months were not interpreted for meteor temperatures for this reason. No data are shown for summer for the radar at this time because sufficiently reliable summertime data were only available for the first time in 2000, and there has not yet been time to analyze these.

One of the most significant points which is clear in these figures is that both the lidar and the meteor data produce temperature amplitudes at 88 km altitude which exceed the estimates for the GSWM model. Nevertheless, we should emphasize that the model concentrates on migratory tides, and does not consider non-migrating tides or zonally symmetric tides. The diurnal phases are all in the range of 3 to 12 h for spring, 0 to 8 h for fall, and −2 to 5 h for winter. Although this represents a moderately large spread, some of the

reasons for this scatter is intraseasonal and interannual variation, as we shall see shortly. The semidiurnal phases show quite good agreement between all techniques in spring and winter, and all three sets of data show quite different results for the phases in fall. However, the temperature amplitudes are also quite low in that season.

Since some of the measurements in Figs. 4 and 5 show noticeable differences in the phases, we have used the much more extensive data set from the Clovar meteor radar at London, Ontario in Canada, (e.g. see Hocking and Thayaparan, 1997) to examine interannual variability. We should note, however, that although the salient features of the Clovar meteor radar have been described by Hocking and Thayapaparan (1997), it has also been significantly upgraded since 1997, and functions more like the SKiYMET radars described in Hocking et al. (2001), with the exception that the data from the five receiving antennas are multiplexed on a pulse to pulse basis successively into a single receiver in a 5-point cycle, rather than being fed to separate receivers. The operating frequency is 40.68 MHz. Data are shown separately for each month of each year during those periods when sufficient data were recorded in the time frame 1997 to 2000.

Both "naive" ("uncorrected") and "true" ("corrected") meteor results are shown in these figures. The true amplitudes can be seen to be generally shifted to the left of the naive values. This is also true in four out of the six cases for Albuquerque in Figs. 4 and 5 (the only exceptions being the diurnal and semidiurnal tides during "fall", and even then the semidiurnal case is barely larger than the naive value). Indeed, the "true" temperature amplitudes are less than the "naive" values in 49 out of 51 cases studied, and the average reduction is about 20%. The variations seen in the figures represent both interannual variability, as well as month to month variability. There is considerable spread, which encompasses the values presented by the GSWM and States and Gardner (2000b).

With regard to diurnal phases (Fig. 6), there is again considerable spread, but generally the median phases overlap quite closely with the results presented by both the GSWM and States and Gardner (2000b). The disparities observed in Figs. 4 and 5 for Albuquerque can be explained as part of the interannual and intraseasonal variability, since the Albuquerque meteor diurnal temperature phases lie within the general scatter region of meteor phases described in Fig. 6. Similar comments apply to Fig. 7.

The largest discrepancies in phases between the different techniques in Figs. 4 to 7 occur for the semidiurnal tide in summer and fall. During these months, the lidar data and the GSWM show approximately oppositely directed phases, and the meteor data support the predictions of the GSWM in both cases slightly more closely. Nevertheless, there is a substantial phase change in the GSWM phases from 85 to 90 km altitude in summer, indicating a possible strong sensitivity to year-to-year variability. It is possible that all the data are representative of the circumstances during which their respective measurements are made, and the differences represent interannual variability. Further investigations are required here.

In Figs. 8 and 9 we present monthly (vector) averages of the meteor temperature tidal values for Albuquerque and London (Ont.), respectively. For comparison, we also show the seasonal results from the GSWM for 36° N, and the lidar results for 40° N. The GSWM and lidar data have been drawn as horizontal lines covering each season. The agreement in diurnal phases is generally fair, and the semidiurnal phases between January and May are generally quite agreeable. The period from July to November shows the biggest phase differences between the lidar and the other two procedures. The data from the Clovar and Albuquerque meteor radars are also in generally good agreement with respect to the phases.

The tidal amplitudes show greater variability at Albuquerque than at Clovar, which is almost certainly an artifact of the fact that the Clovar data have been averaged over a longer time period. Thus, the Clovar data are more representative of "typical" conditions, but the larger values shown in Fig. 8 are still largely representative of the particular months for which these data were acquired. The fact that the tidal amplitudes reach 20 K in November (diurnal) and March (semidiurnal) is a point which needs further investigation. Interestingly, our average tidal amplitudes in Fig. 9 (Clovar) show broadly quite similar values to those recorded by the lidar at Illinois, but both data sets in general show values in excess of the GSWM predictions.

Figure 10 (lower portions) shows comparisons between the phases of the temperature tides and the wind tides. The wind amplitudes are also shown in the upper graphs for reference. It seems clear that the temperature tides are often quite similar to the phases of the meridional winds. Similar results are valid for the Clovar data. We consider this to be a significant result, and in Sect. 5 of this paper we present a theoretical analysis which demonstrates why this correlation occurs. We will also show in that section that we do not expect a one-to-one relationship between the amplitudes of the wind tides and the temperature tides, so the fact that the diurnal temperature tides are quite modest in March and April, but the wind tides are very large, should not be considered as a point for concern.

Figures 11 and 12 show diurnal and semidiurnal tidal parameters for both the winds and temperatures at Resolute Bay, Canada (75° N). The radar operates at a frequency of 51.5 MHz, so the height of peak meteor counts occurs at a lower height than with the other two radars. Also, due to the high latitude, and the large summer to winter temperature variation, the height of maximum meteor counts (which is also the height to which our temperatures apply) varies from 85 km in winter to 88 km in summer.

The meteor radar at Resolute Bay is susceptible to interference from a variety of sources, including other instruments which operate close to it. This is particularly true in winter, when many other optical instruments operate simultaneously. Hence, there are times of the year when we can produce sufficient data to realize tidal winds, but insufficient data to produce good temperature tides. We have also noticed frequent

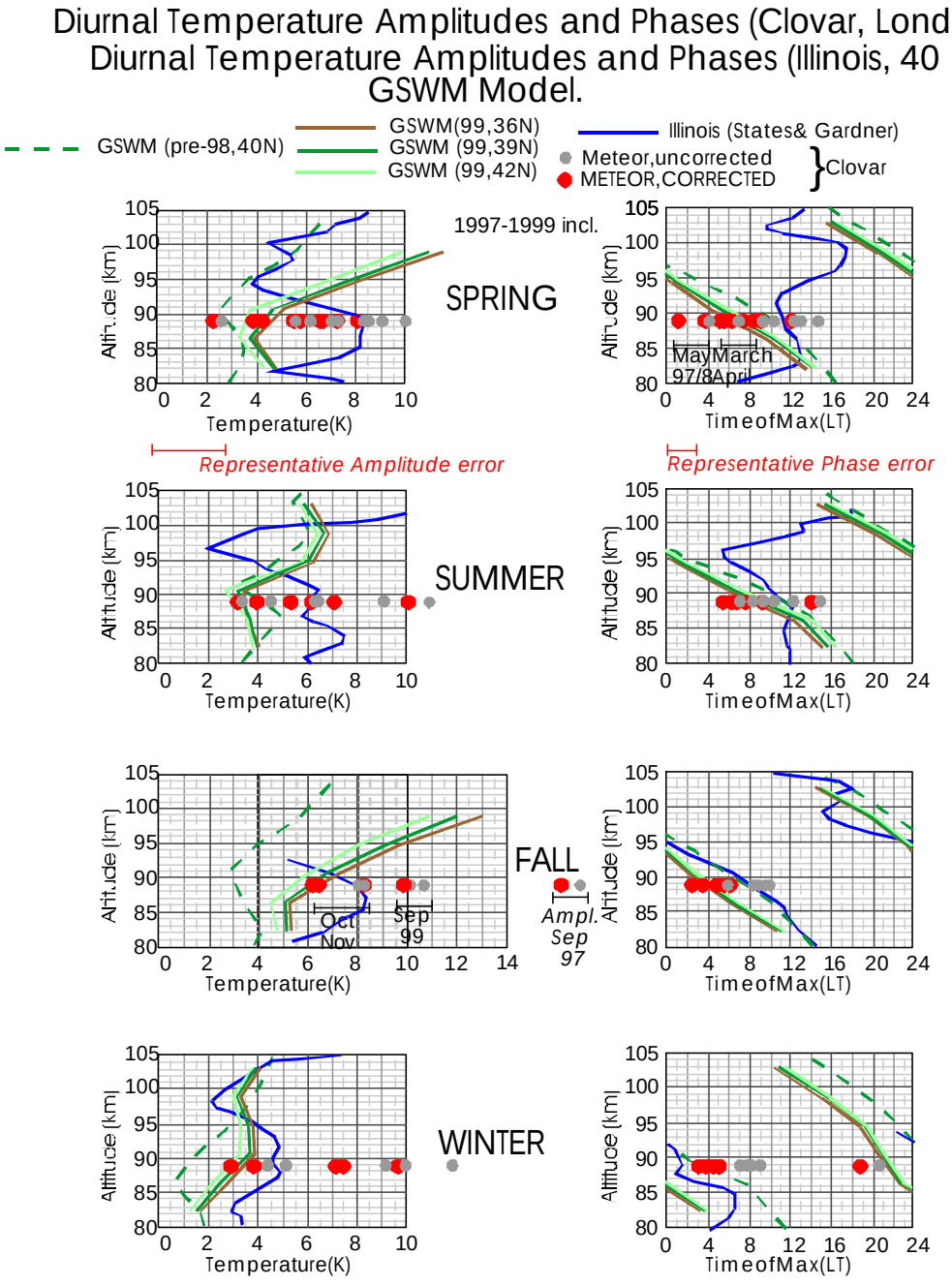

Fig. 6. As for Fig. 4, but in this case the meteor data which are presented are for the Clovar meteor radar at London, Ontario (43° N). Data from several years during the period 1997 to 2000 are shown. In contrast to Fig. 4, however, each month of data has been analyzed and plotted separately, in order to demonstrate the degree of variability that occurs from month-to-month and year-to-year. Note that as a rule the "uncorrected" or "naive" amplitude estimates exceed the "true" (corrected) estimates. Error bars are not given for all points, since it would clutter the diagram too much, but representative error bars are given.

occurrences of large terdiurnal tides at Resolute Bay, as determined by wind measurements, and we chose to avoid analyzing for temperature tides in these months, for reasons described earlier. The observations of these large terdiurnal tides are consistent with observations reported by Sivjee and Walterscheid (1994), Walterscheid et al. (1986), Walterscheid and Sivjee (1996), and Walterscheid and Sivjee (2001).

The wind tides in Figs. 11 and 12 are averages over 6 years of data, although in 1997 data were only available for June and July. A clear annual cycle in amplitudes is apparent, with maxima in both the tidal and semidiurnal components in the equinoxes. We show data for both 85 and 88 km throughout the year. Phases are only shown if the amplitudes exceed

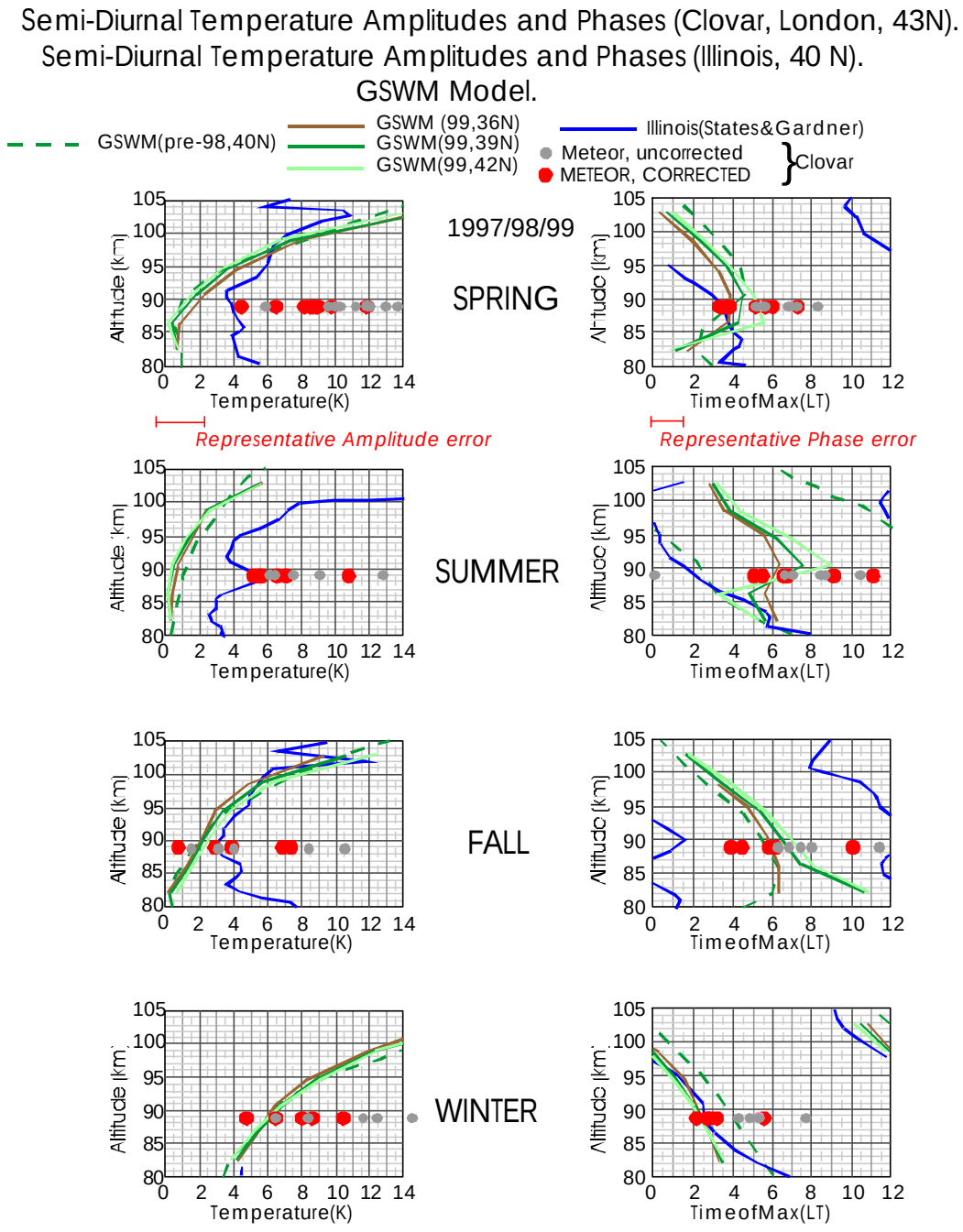

Fig. 7. As for Fig. 6, but for the semidiurnal components.

threshold values of 3 m/s for the diurnal tides and 2 m/s for the semidiurnal tides. The phases are also quite well behaved in most months. A 6-h offset between the zonal and meridional phases is apparent in the diurnal component throughout most of the year, and a 3-h offset between the zonal and meridional components is apparent for the semidiurnal component in the months from August to May.

However, we do recognize that during the summer months, some of this behaviour breaks down. The diurnal tide shows a significant phase change during the month of June, and in some years this can be quite extreme. The 6-h time shift between times of maximum zonal and meridional winds also disappears. With regard to the semidiurnal tide, the oscillation actually becomes linear in June and July, with the phases of the zonal and meridional components becoming almost equal.

With regard to the temperature tides, we have only been able to produce estimates in 6 months, which are shown in Figs. 11 and 12. A summary of the vertical wavelengths used in these determinations can be found in Hocking (2001),

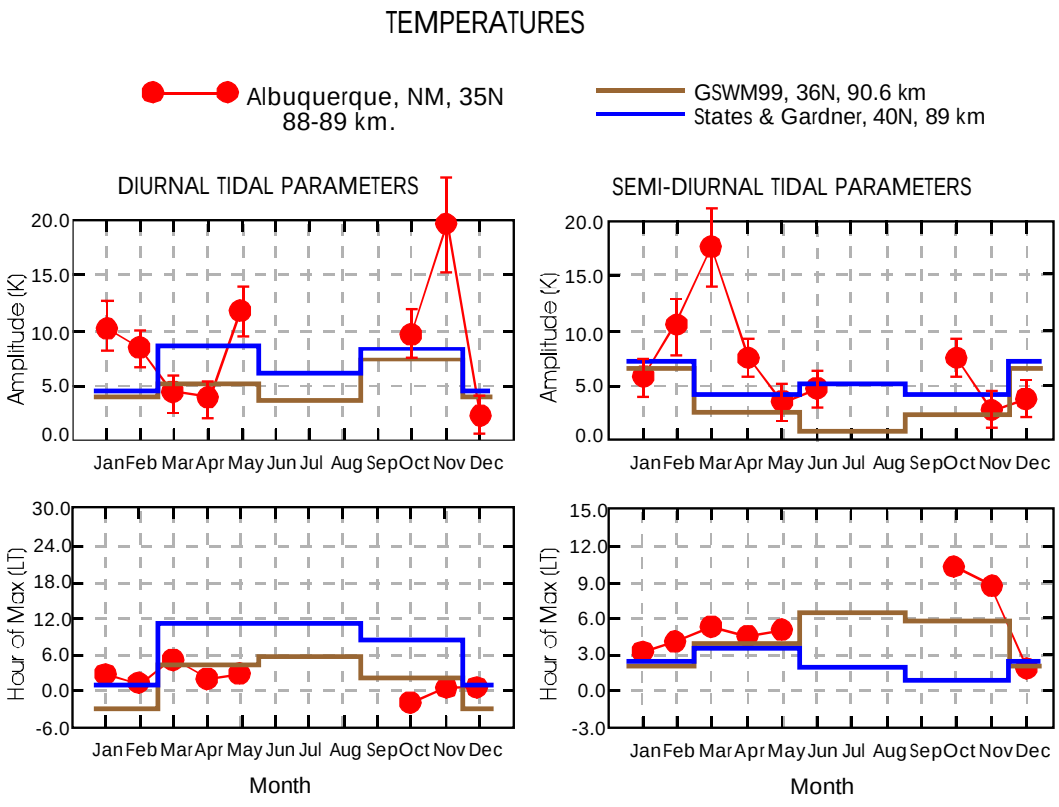

Fig. 8. Meteor temperature tidal parameters plotted as a function of month of the year for 88–89 km altitude for Albuquerque, New Mexico, compared to lidar-derived measurements for Illinois (40° N) and the GSWM for 36° N. The meteor data represent vector averages over all available months in the period 1998 to 2000. Error bars are given for the amplitudes. For the phases (times of maximum), the errors are smaller than the symbols used.

Fig. 4. In the other months, the existence of terdiurnal tides, and in some cases insufficient data quality, have hampered or prevented our temperature retrievals.

The first point from these figures regarding temperature tides is that in general the diurnal temperature tide dominates over the semidiurnal tide. The semidiurnal tides are in general of modest amplitude, being about 2 K in June, September and December, and 5 K in January and May. These small values are consistent with the predictions of the GSWM, although that model often predicts even smaller values (less than 1 K). A larger value of 12 K is evident in March, and this large value is something of an exception. The phases of the semidiurnal tide (Fig. 12) show a general tendency to follow the phases of the meridional winds, broadly consistent with our observations at Albuquerque and London (e.g. Fig. 10).

On the other hand, the diurnal tides often show amplitudes of 10 K and more, and these are completely different from the predictions of the GSWM, which generally predicts values of 2 K and less. Furthermore, the phases of the temperature tides are often quite different to those of either the zonal or meridional winds. In June, the phase of the diurnal temperature tide changes substantially relative to the preceding months. Further studies of the summertime tidal phenomena are clearly needed, but the lack of correlation between the wind and temperature phases is quite obvious.

The significant differences between the temperature diurnal tidal phases and the phases of the zonal and meridional winds is a very important result. It suggests that the wind tides and the temperature tides may be associated with different modes of propagation, and we will return to this point later.

4 Observations with meteorological rockets

Since some of our tides seem to be larger in amplitude than the predictions for migrating tides, as proposed by the Global Scale Wave Model (GSWM) of Hagan et al. (1999), we seek validation of our large tidal amplitudes, particularly at the Resolute Bay site. We have tried to examine other sources of data for temperature amplitudes. One recent data set is that of Chen et al. (2000). These authors also used a lidar for their studies, similarly to States and Gardner (2000b), and observed over 18 periods covering 24 h. Although they observed that the mean nighttime temperatures averaged over a full year were only 2–3 K different from the mean daytime temperatures averaged over a whole year; on any one day temperature variability of 10–20 K from day to night was

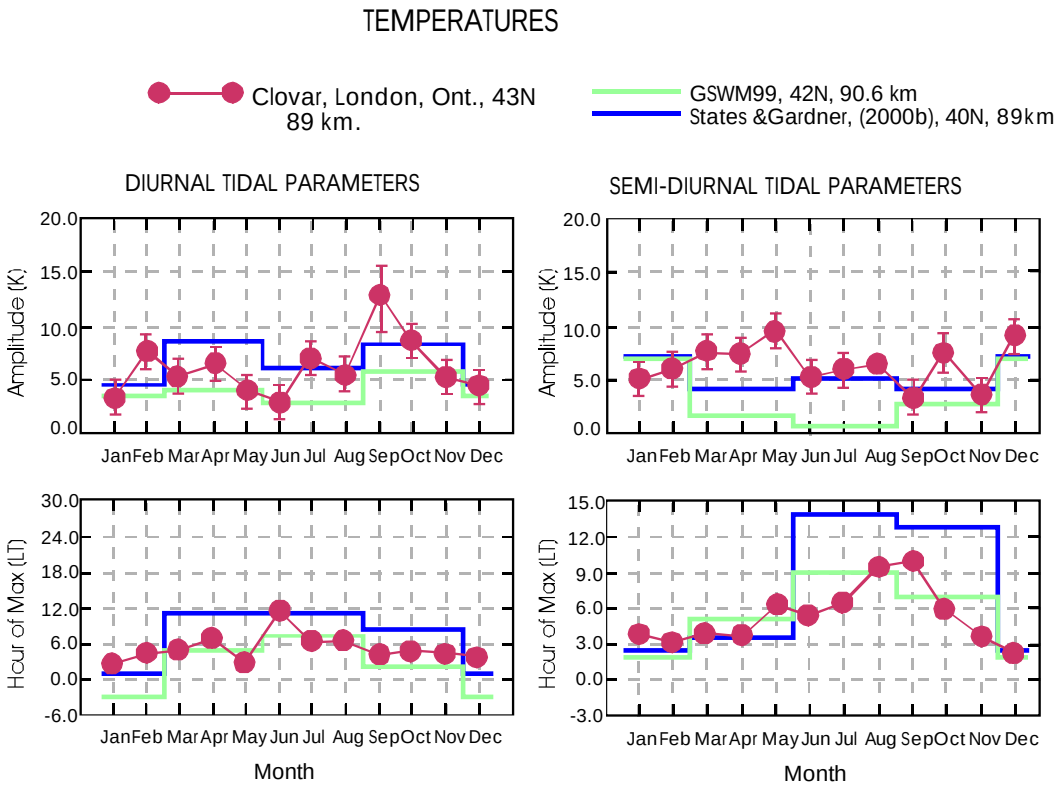

Fig. 9. As for Fig. 8, but for the Clovar meteor radar at London, Ontario, Canada.

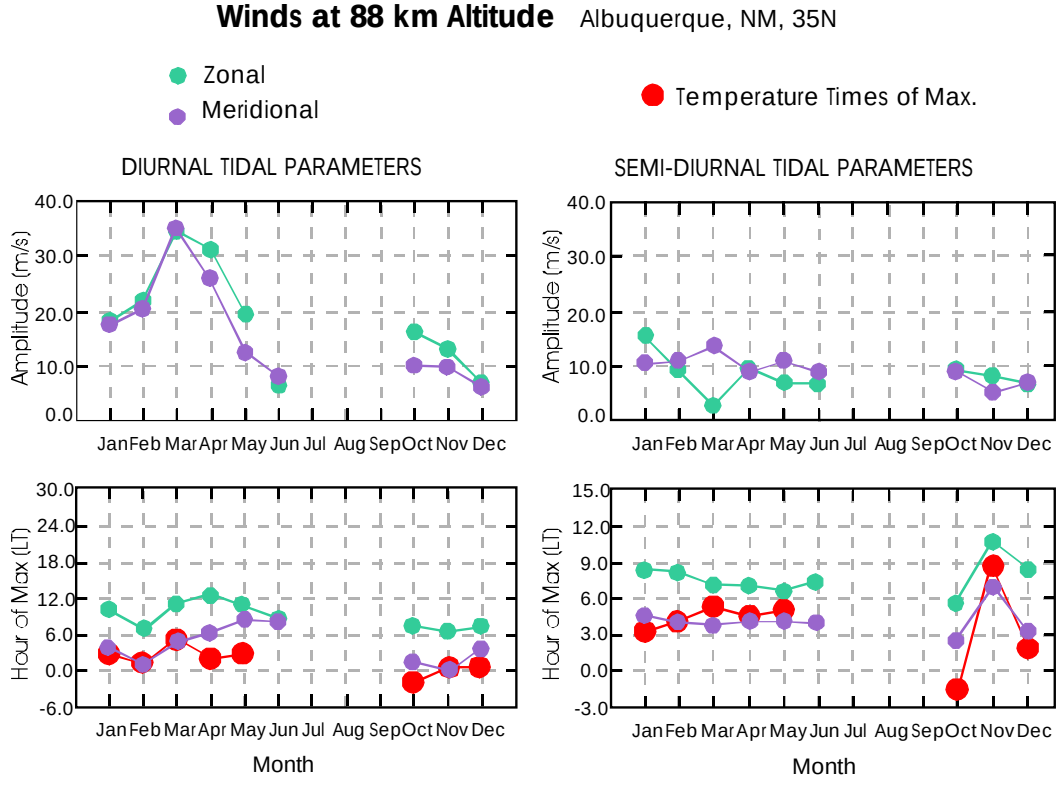

Fig. 10. Comparison between wind and temperature tidal phases (lower plots) for Albuquerque. The amplitudes of the wind tides are also shown for reference. In each case the errors are comparable to or smaller than the sizes of the symbols.

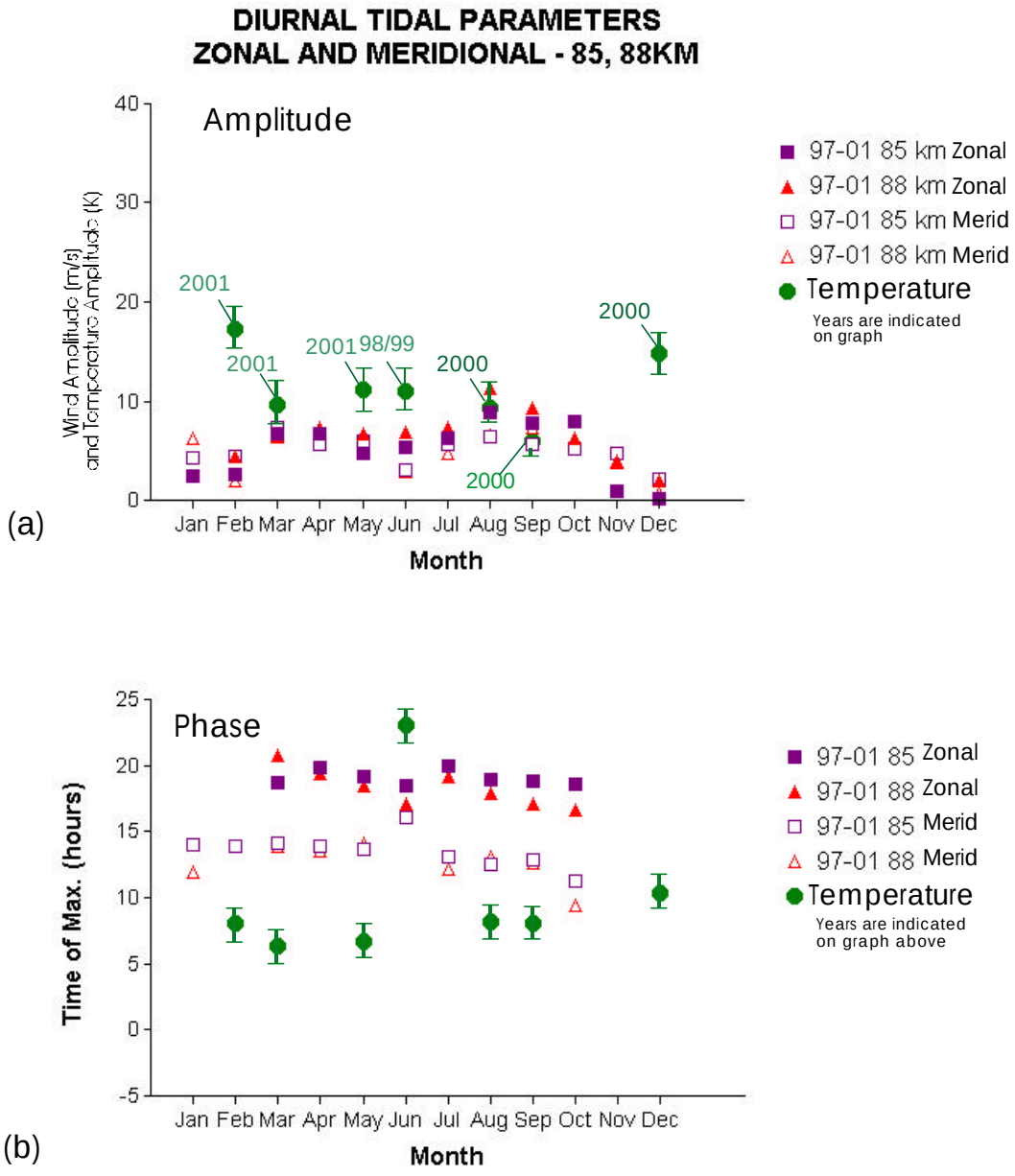

Fig. 11. Tidal parameters deduced by the meteor radar at Resolute Bay, Canada (75° N). These graphs include both wind and temperature diurnal temperature parameters. The wind data represent vector averages for each month, with useful data over the period 1997 to 2001. Due to poorer data rates, and in some cases the existence of terdiurnal tides, it has not always been possible to deduce the temperature tides, so only data for selected months in selected years are shown. The wind data are shown for both 85 and 88 km altitude, while the temperature data are shown for the height of peak meteor detection (typically 85 km in winter and 88 km in summer for this 51.5 MHz radar).

often visible. This can be seen in several examples in their Fig. 1.

Another very useful source is the large database of rocket observations produced in the 1970's and 1980's at a variety of sites worldwide (e.g. see Eckermann et al. (1995) and references therein). Unfortunately, these vehicles generally only reached a ceiling of about 70 km or less, so we cannot make direct comparisons with our own data, but we can make some general observations which support the large tidal amplitudes that we have found.

In order to make useful tidal studies using rocket data, we have binned all the data from a variety of sites according to local time of day. The data cover several years, and also incorporate substantial interannual variability. The data also suffer from the fact that rocket launches generally took place in daylight hours, and especially between 8 am and 6 pm. For some stations, this concentration of flights was so tight that it was impossible to extract diurnal cycles of any sort.

Nevertheless, it was possible to find some sites with sufficient daily coverage to give some clues about expected diurnal variations. Some of these examples are shown in Fig. 13. Note that we have grouped data from several months, in or-

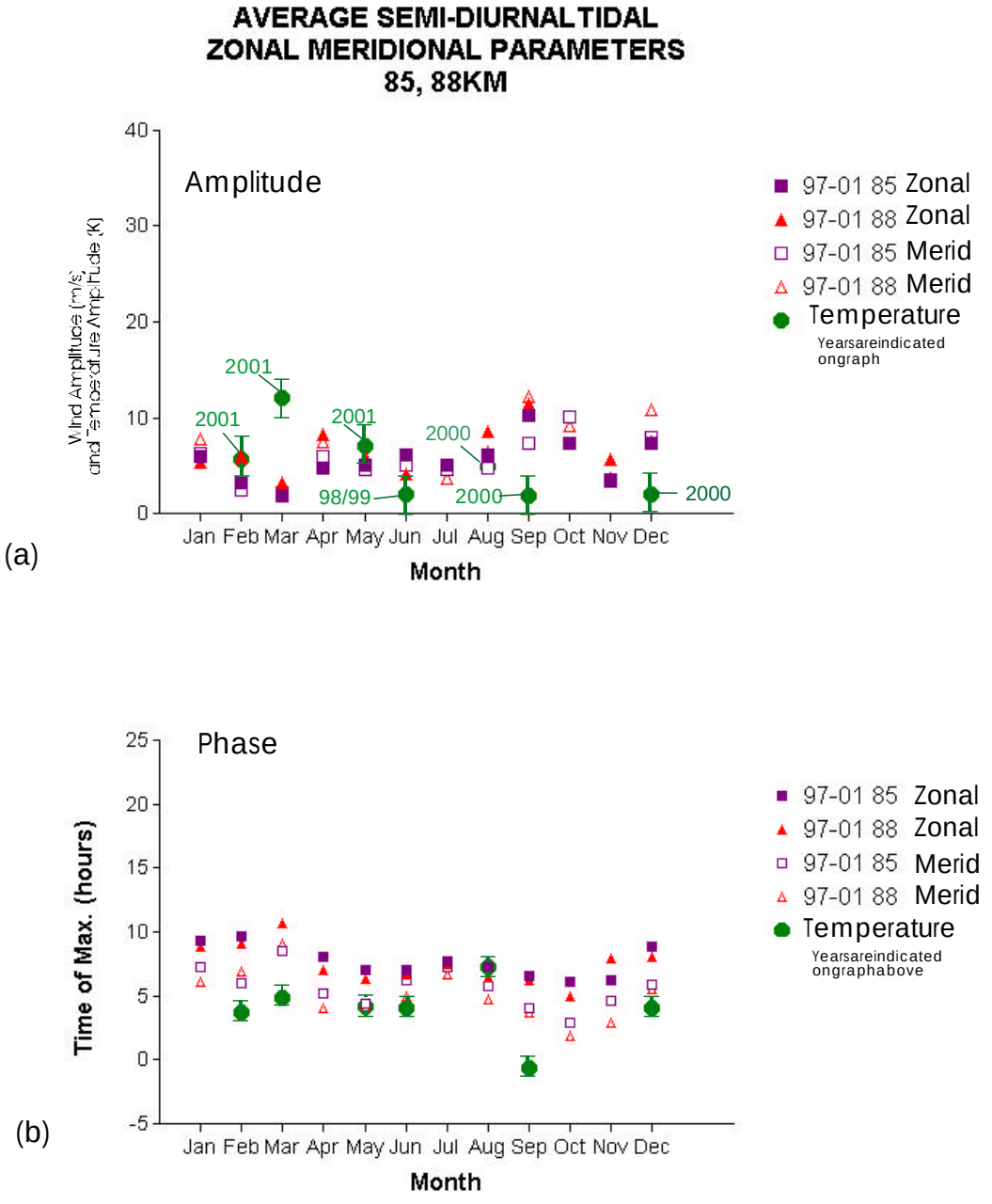

Fig. 12. As for Fig. 11, but for the semidiurnal component for Resolute Bay.

der to produce sufficient data quantities so that we can make meaningful observations. It must be remembered that these data were recorded at heights below 70 km altitude, so they do not represent data at 85–90 km. However, we expect that the tides will generally grow with increasing height, so fluctuations observed at these lower heights will be amplified at higher heights. Hence, we consider that amplitude fluctuations shown here will be underestimates for data at 85–90 km altitude.

Although not entirely definitive, it does appear that some of these sites show noticeable diurnal cycles, which we interpret as tides. For example, Ascension Island shows a tendency for maxima of about 235–240 K at 13:00–14:00 LT, and minima of about 215 K towards midnight. This could represent a diurnal tide with an amplitude of over 10 K. Primrose Lake, which is a moderately high-latitude site, shows a diurnal cycle varying from minima of about 240 K at 04:00 and 15:00–16:00 LT, to maxima in between these times. This partial oscillation could possibly be part of a semidiurnal cycle. Maxima are of the order of 260 K, so a semidiurnal temperature tide of the order of 10 K is again indicated.

Chatanika actually shows a quite good coverage of local times, but there is still a concentration around noon. However, for the period from August to December, evidence of a diurnal cycle exists at 45–55 km, with maxima around noon and minima around midnight. A diurnal tide with an

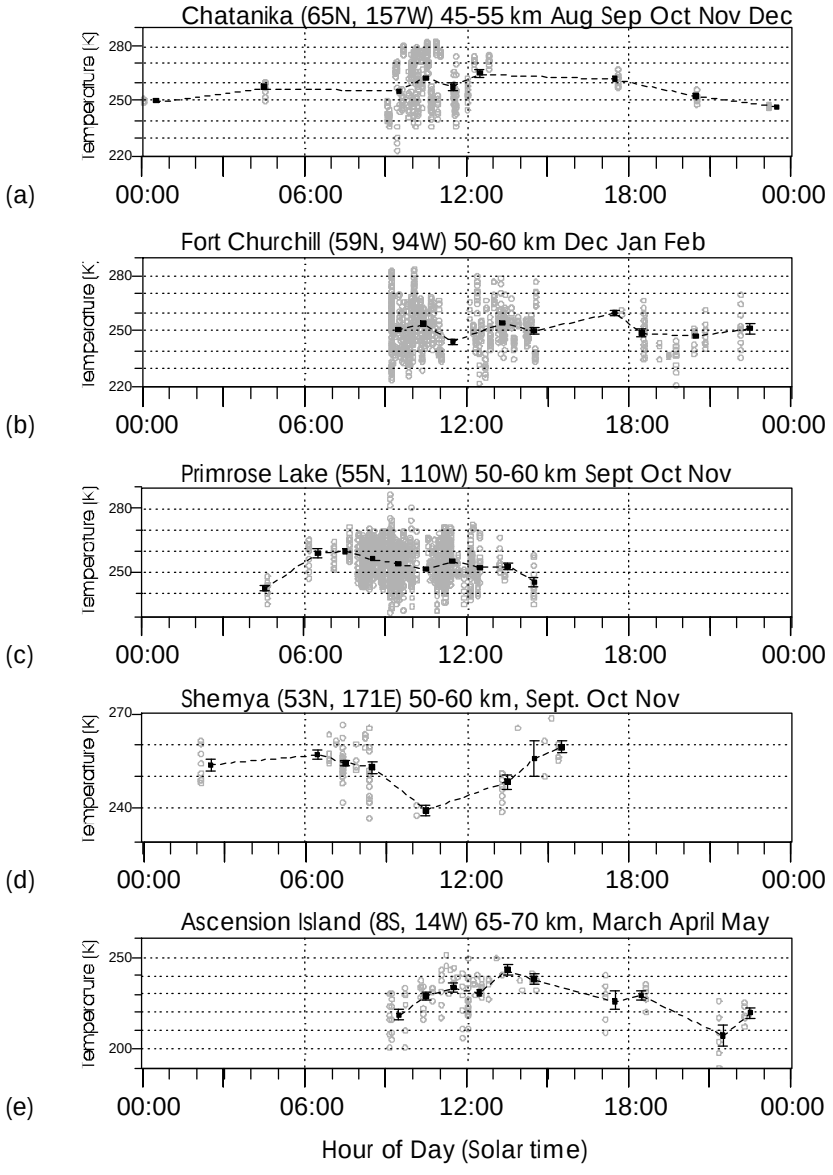

Fig. 13. Superposed epoch (composite day) graphs of rocket temperatures in the 40 to 70 km altitude range deduced at various rocket sites in the late 1970's and early 1980's. Light circles represent raw data, while dark squares represent hourly averages. Error bars illustrate the standard deviations for the means. Where no error bar is shown, it indicates that the error bars are smaller than the size of the square symbol used to represent the mean.

amplitude of the order of 5–7 K is indicated.

At Shemya, a large diurnal variation is indicated, but the data are few in number, and we are not sure about the significance level of these data. The data for Fort Churchill do not show a smooth diurnal variation, although variations from maxima to minima are of the order of 15 K.

Hence, although these rocket data are often sparse at critical times, and are averaged over large numbers of years, and cover height regions below our area of interest, they are sufficient to indicate that tidal amplitudes of the order of 10 K do exist, even as low as 70 km in altitude. Larger amplitudes will exist at higher altitudes. The rocket results also support the observations of States and Gardner (2000b), which also indicate tidal amplitudes in excess of the predictions of the GSWM.

5 Temperature and wind phases

Although we have shown that our phase results at mid-latitudes are generally in agreement with the GSWM (1999), it is also instructional to examine whether our results are consistent with more fundamental arguments. One observation which seems to be somewhat robust, and which can serve as a useful extra test of the validity of our observations, is the recognition that the temperature phases and the phases of the meridional wind seem to be very similar. We will now show

that this result is to be expected for mid-latitude diurnal and semidiurnal tides, using a beta-plane approximation.

We begin with the v' component of the force equation, and assume solutions u', v', w' and T' of the type $\Phi' = \Phi'_0 e^{i(kx+mz-\omega t)}$, where x is directed eastward, z is vertical, u' is the eastward velocity, v' is the northward velocity, and w' is the vertical velocity. Then

$$\frac{D}{Dt}v' = -\frac{1}{\rho}\frac{\partial p'}{\partial y} - fu', \tag{17}$$

where f is the Coriolis parameter. Substituting variables of the form $\Phi' = \Phi_0 e^{i(kx+mz-\omega t)}$ and ignoring the pressure fluctuation terms for now then gives

$$-i\omega v' + iku'v' + \frac{\partial v'}{\partial y}v' + imw'v' = -fu'. \tag{18}$$

Dividing through by ω, and recognizing that $C_x = \frac{\omega}{k}$ is the horizontal phase speed, and $C_z = \frac{\omega}{m}$ is the vertical phase speed, then

$$-iv' + i\left(\frac{u'}{C_x}\right)v' + \frac{1}{\omega}\frac{\partial v'}{\partial y}v' + i\left(\frac{w'}{C_z}\right)v' = -\frac{f}{\omega}u'. \tag{19}$$

The horizontal phase speed is several hundred metres per second (circumference of the Earth at the latitude of interest divided by the wave period), so provided u' and v' are less than of the order of 50 ms^{-1}, and $C_z \gg w'$, and assuming for now that v' changes slowly with increasing latitudes such that $\frac{\partial v'}{\partial y} \ll \omega$, then we are left with the well-known result that

$$u' = i\frac{\omega}{f}v', \tag{20}$$

i.e. the zonal and meridional components should be in phase quadrature. However, these equations have made the assumptions implicit in this derivation clear, and if any one of the previously mentioned assumptions breaks down, the phase quadrature may well be lost. We wish to determine if similar phase relationships can be derived between the temperature and winds phases.

We wish to examine the temperature at a fixed height z. Temperature changes will occur as parcels of air from underlying or overlying air that is moved adiabatically to this height. If a parcel of air is displaced vertically in such a manner, it will change temperature relative to its surroundings by an amount T', where

$$T' = -\left[\Gamma_a - \Gamma_e\right]\zeta', \tag{21}$$

with ζ' being the vertical displacement of the parcel. Γ_a is the adiabatic lapse rate and Γ_e is the environmental (background) lapse rate, which equals $-\left(\frac{dT}{dz}\right)_{background}$. We also note that $w' = \frac{d\zeta}{dz}$, so that $\zeta' = \frac{w'}{-i\omega} = i\frac{w'}{\omega}$. Finally, we also recall that the Brunt-Vaisala frequency is equal to $N = \sqrt{\frac{g}{T}\left[\Gamma_a - \Gamma_e\right]}$.

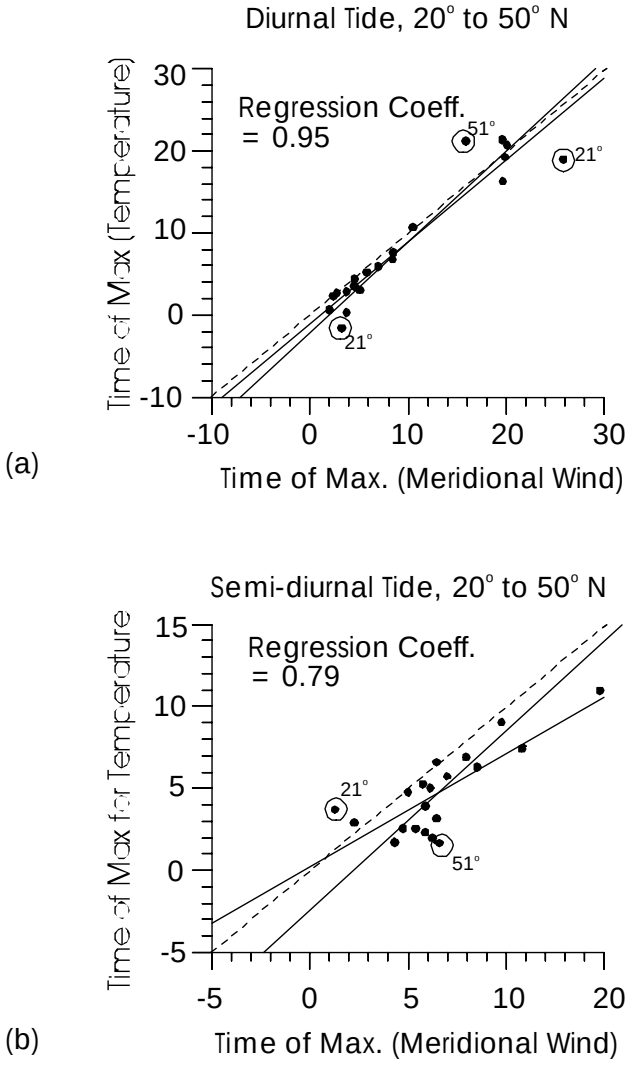

Fig. 14. Scatter plots of the phases of the temperature tides vs. the phases of the meridional winds as determined from the GSWM for the latitude band 20° N to 50° N for **(a)** the diurnal and **(b)** the semidiurnal tides. The origin of some of the outliers are also indicated. In each case the broken line indicates the 1:1 line, and the solid lines represent least-squares fits of the regression of the abscissa on the ordinate, and the ordinate on the abscissa.

Hence, the temperature perturbation due to the tide at a fixed height is

$$T' = -i\frac{N^2 T}{g}\frac{w'}{\omega}. \tag{22}$$

Finally, we will employ the continuity equation

$$\frac{D\rho}{Dt} + \rho\left(\nabla \cdot \boldsymbol{u}\right) = 0. \tag{23}$$

When we substitute the usual perturbation terms we obtain

$$-i\omega\frac{\rho'}{\rho} + iku' + \frac{\partial v'}{\partial y} - \frac{w'}{H} + i\boldsymbol{m}w' = 0, \tag{24}$$

where H is the atmospheric density scale height (e.g. see Walterscheid and Hocking, 1991). We recognize that $\boldsymbol{m}$ is a complex number and write that $\boldsymbol{m} = m_R + im_i$, where $m_i = -\frac{1}{2H_w}$, with H_w being the energy scale height of the wave. For non-dissipating waves, $H_w = H$. For dissipating waves, $H_w > H$ or $H_w < 0$.

If we assume that the wave has downward phase velocity (upward energy propagation), we may write $\boldsymbol{m} = -\frac{2\pi}{\lambda_z} - \frac{i}{2H_w}$. We also utilize the relation $\frac{\rho'}{\rho} = -\frac{T'}{T}$ and apply Eq. (20) and Eq. (22) to give

$$\left(\frac{1}{v'}\frac{\partial v'}{\partial y} - \frac{\omega}{f}k\right)v' + \frac{g\omega}{N^2}\frac{T'}{T}\left[\frac{2\pi}{\lambda_z} + i\left(\frac{N^2}{g} + \frac{1}{2H_w} - \frac{1}{H}\right)\right] = 0. \quad (25)$$

Notice we have retained all terms, and have not employed the anelastic approximation. Indeed application of the anelastic approximation degrades the correlation of which we will discuss shortly. Assuming that v' varies only slowly in phase with latitude, the term $\frac{1}{v'}\frac{\partial v'}{\partial y}$ will be almost purely real. We will call this quantity γ, and assume that it is purely real. If we define κ to equal $\frac{\omega}{f}k - \left(\frac{1}{v'}\frac{\partial v'}{\partial y}\right)$, then

$$T' = \frac{\kappa N^2 T}{g\omega}\left[\frac{2\pi}{\lambda_z} + i\left(\frac{N^2}{g} + \frac{1}{2H_w} - \frac{1}{H}\right)\right]^{-1} v'. \quad (26)$$

We need to investigate the sign of κ. For migrating tidal oscillations, the angular frequency is $n\Omega$, where Ω is the angular rotation rate of the Earth, and $n = 1$ corresponds to a diurnal tide, $n = 2$ corresponds to a semidiurnal tide, and so forth. At latitude θ, the Coriolis parameter is $f = 2\Omega\sin(\theta)$. At latitude θ, the wave number k equals $2\pi n/(2\pi r_E\cos\theta)$, where r_E is the radius of the Earth. Hence,

$$k\frac{\omega}{f} = \frac{n^2}{r_E\sin(2\theta)}. \quad (27)$$

Regarding the term $\gamma = \frac{1}{v'}\frac{\partial v'}{\partial y}$, we will consider primarily the first and second order modes. The S_1^1 mode, for example, peaks at mid-latitudes, and falls away towards the poles, and possibly the equator. A crude estimate of the typical magnitude of this quantity can be found by assuming that the mode falls away approximately linearly from about 30°N to the poles, covering, say, two-thirds of the distance from the equator to the poles in the process. Thus the horizontal distance covered is about one-sixth of the Earth's circumference, or approximately one Earth-radius. If we consider the situation about half way between the maximum and the poles, then v' is about one-half of the value where the tide maximizes – which we will call v'_{max}. Then, $\frac{1}{v'}\frac{\partial v'}{\partial y} \approx \frac{2}{v'_{max}}\frac{(v'_{max}-0)}{r_E}$, or about $\frac{2}{r_E}$. This is comparable to the expression in Eq. (27), and, therefore, we must retain this term in all of our calculations.

We assumed above that the amplitude v' falls away linearly from it maximum, but this is not the case, and in fact maximum is quite broad, with relatively small slope as a function of latitude (and hence, as a function of y). Thus, in mid-latitudes we expect the term $k\omega/f$ to exceed γ, and, therefore, expect κ to be positive. At higher latitudes, where γ may exceed $k\omega/f$ due to small values for v' and larger gradients $\frac{\partial v'}{\partial y}$, κ, γ will be negative and will reinforce $\frac{\omega}{f}k$. However, it is possible at low latitudes, where $\frac{\partial v'}{\partial y}$ is increasing, that it may cancel and overcome $\frac{\omega}{f}k$, so in those cases the phase could reverse sign by 180°. But at mid-latitudes, and wherever the tidal wind amplitude is decreasing towards the poles, or is positive and weak, we expect κ to be positive.

We now need to consider the term $\left[\frac{2\pi}{\lambda_z} + i\left(\frac{N^2}{g} + \frac{1}{2H_w} - \frac{1}{H}\right)\right]$ in Eq. (26). We consider some special cases. If the scale height H is of the order of 7 km, and H_w is also 7 km (non-dissipating tide), and N^2 is about $1 - 2\times10^{-4}$ (Brunt-Vaisala period between 5 and 7.5 min), then the imaginary component is about $-(5$ to $6)\times10^{-5}$. If the vertical wavelength is short, as with the S_1^1 mode, say, 25 km, then $2\pi/\lambda_z$ is about 2.5×10^{-4}. Thus the real part dominates by a factor of about 4 to 5. Numerically, Eq. (26) becomes $T' \simeq 4\times10^3\frac{\kappa N^2 T}{g\omega}\times e^{i\varphi}$, where $\varphi \simeq .19$ radians, corresponding to a phase difference of about 0.75 h. Hence, in the case of short vertical wavelengths and the diurnal tide, the temperature tide and the meridional velocity should have similar phases to within an hour or two. Even for vertical wavelengths of the order of 50 km, the phase difference is less than 1.5 h. In the case of the semidiurnal tide, the imaginary term remains as above, but the vertical wavelengths are often in the range above 80–100 km, so the real part can become of the order of 6×10^{-5}. Even in this case, however, the phase differences are less than 45° (3 h for the diurnal tide, 1.5 h for the semidiurnal tide).

Hence, if the tidal vertical wavelengths are moderately short (less than about 80 km for either the diurnal or semidiurnal component), we generally expect that the temperature oscillations will be almost in phase with the meridional oscillations. This will be true at mid-latitudes and any location where $\frac{\partial v'}{\partial y}$ is less than zero in the Northern Hemisphere. In the Southern Hemisphere, the same is true at mid-latitudes, as well as any place where $\frac{\partial v'}{\partial y}$ is greater than zero (the sign having changed as a result of the fact the f is negative in the Southern Hemisphere).

We have used the GSWM (Hagan et al., 1999) to check our assertions. Figure 14a shows a scatter plot of temperature phases vs. meridional wind phases for latitudes from 20° N to 50° N, and the correlation is clearly very good. The three main outliers (marked on the graph) arrive from points at 21° N and 51° N. Thus, our theory is well confirmed, and supports our observations from our radar, which frequently show that the temperature and meridional wind phases match. Figure 14b shows the same calculations for the semidiurnal component, and again the correlation is very good for these mid-latitude sites, although the scatter is a

little worse than for the diurnal tide, and there is a mean phase offset.

Finally, we should consider the case that the vertical wavelength becomes infinite. In this case, $\frac{2\pi}{\lambda_z}$ is zero, and the denominator of Eq. (26) is purely imaginary. Substitution of Eq. (20) into Eq. (26) makes it clear that in these cases, T' should be in phase with the zonal wind, u', provided that $\left(\frac{N^2}{g} + \frac{1}{2H_w} - \frac{1}{H}\right)$ is less than zero. A heavily dissipating tide could have H_w less than zero, but this would make this term even more negative. Only if $\frac{N^2}{g}$ becomes very large do we expect the phase of the temperature tide to reverse and shift 180° out of phase with the zonal wind.

Hence, the two extreme cases of short vertical wavelengths (up to 80 km or so) and infinite vertical wavelengths produce temperature phases close to those of v' and u', respectively, provided that $\kappa > 0$ (Northern Hemisphere). Tides with moderately long wavelengths (greater than 100 km), but not infinite ones, may have a phase which lies between those of u' and v'. Thus, at mid-latitude and higher, we expect the phase of the temperature tide to lie between the phases of the meridional and zonal winds. This result is not robust, since it depends on the sign of κ, but our calculations suggest that it should be true for much of the time. We note that in the graphs for Albuquerque, shown in Fig. 10, there is indeed a tendency for this rule to be followed. Similar results apply for the Clovar radar. Thus, our results are consistent with expected theory regarding phases. The frequent agreement with the GSWM has also been noted and gives further confirmation that our results are reasonable.

We should also consider the amplitudes that we have observed. If we consider Eq. (27) and Eq. (26), we can deduce some idea about typical expected temperature amplitudes. To begin, consider the diurnal S_1^1 tide, and let us take T to be 200 K, N^2 to be 2×10^{-4}, and H to be about 7 km. We will also assume that the terms $\frac{\omega}{f}k$ and $\frac{1}{v'}\frac{\partial v'}{\partial y}$ contribute approximately equally to κ, and that they add in magnitude (requiring that v' be decreasing towards the poles). Then $\kappa \simeq 2\frac{n^2}{r_E \sin(2\theta)}$, from Eq. (27). If we take $\theta \simeq 40°$, then from Eq. (26) we produce $T' \simeq 3 \times 10^{-6}\lambda_z v'$. For $\lambda_z = 25$ km, and $v_0' = 20\,\mathrm{m\,s^{-1}}$, $T_0' \simeq 1.5$ K. Note that this will not apply for evanescant modes. We might expect values of 2–3 times this if the latitudinal gradient of v' is stronger and more negative in the Northern Hemisphere, and somewhat less if the latitudinal gradient of v' is positive. Longer wavelengths can also increase T'. Thus, we could expect values for T' as high as 6–9 K in regions with vertical wavelengths of 50 km. Higher order tidal modes may have larger wavelengths and larger values for κ. Hagan et al. (1999) seem to suggest that maximum values should normally be around 6–8 K at 90 km altitude (e.g. see Fig. 6, "fall"), and "typical values" should be of the order of 2–5 K, and these results are not inconsistent with our theory.

For the semidiurnal tide, κ will often be even larger than for the diurnal tide, especially due to the n^2 dependence in Eq. (27). The temperature fluctuations will be further enhanced by the longer wavelengths associated with semidiurnal tides. From Fig. 7, typical semidiurnal tidal amplitudes should be in the range of 2–6 K.

6 Discussion

Our observations of tidal phases are broadly in agreement with expectations, particularly regarding phases. However, our observations show amplitudes as large as 10 K and higher, whereas our calculations, and the model of Hagan et al. (1999) suggest that values should be generally less than about 6 K for migrating tides. We need to understand why our values are this big. As shown, both our results and lidar results (States and Gardner, 2000b) show amplitudes in excess of those predicted by the GSWM. We have also demonstrated that some earlier rocket examples show similar amplitudes at lower heights.

The only factors which can allow the amplitudes to increase, according to our theory in the last section, are increases in N^2 or increases in κ. If the velocity gradient as a function of latitude is large and of the correct sign, κ can be increased by 2–3 times over our expected values. If, in addition, N^2 increases above our expected value, as it may when the temperature gradients become large, we might expect some local enhancement. However, our large amplitudes seem to persist on a continuous basis, so do not appear to be due to local temporal enhancements.

The problem is especially acute in the polar regions. We cannot currently fully explain these large values. Possible explanations for them have been offered by Walterscheid and Sivjee (1996, 2001), Walterscheid (1981) and Hagan et al. (1999). Walterscheid and Sivjee (2001) have suggested that zonally symmetric tides may be important, especially because they are not required to approach zero temperature amplitude at the poles. Wind fluctuations, on the other hand, are bound to approach zero amplitude at the poles. Walterscheid (1981), Fritts and Vincent (1987), Liu and Hagan (1998) and Liu et al. (2000) have proposed that gravity wave modulation by the tide may produce an enhanced artificial tide at levels above the modulation region. However, it is not clear that this could produce a tidal magnification of a factor of 2 or 3. Other non-migratory tides also need to be considered.

Alternate mechanisms also need to be investigated. We have largely assumed that all temperature tides occur as a result of adiabatic compression and expansion of air parcels which are driven vertically by the tides. The possibility must be examined that diabatic processes (possibly associated with chemical heating and cooling reactions) could also introduce temperature fluctuations, which either amplify existing tides or directly introduce new tidal motions in situ.

7 Conclusions

In this paper, we have presented the underlying theory which permits meteor radars to be used to determine temperature

tides in the altitude region around 90 km. The following points are noted.

1. A "composite day" approach may be used to determine diurnal and semidiurnal temperature tides, but important corrections are needed to compensate for the fact that the temperature gradient also varies throughout the day in a tidal manner. It is also necessary to have information about the relevant vertical wavelengths in order to apply this procedure. These values must be obtained from meteor winds. Results obtained without this temperature correction generally overestimate the amplitudes by about 20%, and can result in phase errors of 1–3 h. The correction is less important for tides with long vertical wavelengths. The theory can be extended to include terdiurnal temperature tides, but becomes subject to significant uncertainties in that case, and we have decided not to analyze data with significant terdiurnal wind components.

2. Comparisons with lidar data and the GSWM show broadly similar features regarding phase in most months, with the exceptions of the summer and fall semidiurnal tidal phases, where the GSWM data and the meteor data show different values to the lidar data. Significant interannual and intraseasonal variability is also apparent (Figs. 6 and 7).

3. Theory, experiment and model results suggest that at mid-latitudes, the phase of the temperature tide and the meridional wind should be very similar when the tidal wavelengths are modest (less than about 50–80 km). When the tidal modes become evanescant, the temperature tide and the zonal wind become very similar in phase. This result holds only for downward propagating phase velocities. It also can have errors at high and equatorial latitudes.

4. The relation between the temperature tidal amplitudes and the wind tidal amplitudes depends on the latitudinal gradient of the velocity amplitude, the vertical wavelength of the tide, and also on the value of the wind tide itself. Thus, a monotonic relationship between the wind and temperature tides should not be expected. The temperature tide can be considerably amplified if the latitudinal gradient of the wind amplitude is large in magnitude and the amplitude is decreasing towards the poles.

5. Our tidal temperature magnitudes tend to be greater than those predicted for migratory tides, but earlier rocket studies suggest that such large values are not unreasonable. This implies that models need to include other types of tides, including non-migratory and zonally symmetric tides, and may also need to consider diabatic processes, in order to more properly represent the true temperature tides in the atmosphere.

6. It appears that the diurnal modes that dominate the wind tides in the polar regions are not the same modes as those that dominate the temperature tides, and this accounts for the fact that the diurnal temperature tides and the wind tides have quite different phases for the diurnal component. This is consistent with observations of Walterscheid and Sivjee (2001), who have recognized that zonally symmetric tidal modes must have velocity fluctuations which approach zero at the poles, but that there is no similar constraint on the zonally symmetric temperature tides; thus, zonally symmetric temperature tides can maintain significant amplitudes right up to the poles themselves.

Acknowledgements. The Clovar and Resolute Bay radars used in these studies were constructed with support from the Natural Sciences and Engineering Research Council of Canada. The SKiYMET radar at Albuquerque, New Mexico, is wholly owned by Mardoc Inc., and the data are leased to the University of Western Ontario. Helpful discussions with Richard Walterscheid and Maura Hagan are gratefully acknowledged.

Topical Editor M. Lester thanks two referees for their help in evaluating this paper.

References

Bevington, P. R.: Data reduction and error analysis for the physical sciences, McGraw-Hall, New York, 1969.

Chen, S., Hu, Z., White, M. A., Chen, H., Krueger, D. A., and She, C. Y.: Lidar observations of seasonal variation of diurnalmean temperature in the mesopause region over Fort Collins, Colorado, (41° N, 105° W), J. Geophys. Res., 105, 12 371–12 379, 2000.

Eckermann, S. D., Hirota, I., and Hocking, W. K.: Gravity wave and equatorial morphology of the stratosphere derived from long-term rocket soundings, Q. J. Roy. Meteorol. Soc., 121, 149–186, 1995.

Fritts, D. C. and Vincent, R. A.: Mesospheric momentum flux studies at Adelaide, Australia: Observations and a gravity wave/tidal interaction model, J. Atmos. Sci., 44, 605–619, 1987.

Hagan, M. E., Forbes, J. M., and Vial, F.: On modeling migrating solar tides, Geophys. Res. Letts., 22, 893–896, 1995.

Hagan, M. E., Burrage, D. M., Forbes, J. M., Hackney, J., Randel, W. J., and Zhang, X.: GSWM-98: Results for migrating solar tides, J. Geophys. Res., 104, 6813–6828, 1999.

Hocking, W. K., Thayaparan, T., and Jones, J.: Meteor decay times and their use in determining a diagnostic mesospheric temperature-pressure parameter: Methodology and one year of data, Geophys. Res. Letts., 24, 2977–2980, 1997.

Hocking, W. K. and Thayaparan, T.: Simultaneous and co-located observation of winds and tides by MF and Meteor radars over London, Canada, (43° N, 81° W) during 1994–1996, Radio Sci., 32, 833–865, 1997.

Hocking, W. K.: Temperatures using radar-meteor decay times, Geophys. Res. Letts., 26, 3297–3300, 1999.

Hocking, W. K., Fuller, B., and Vandepeer, B.: Real-time determination of meteor-related parameters ultilzing modern digital technology, J. Atmos. Solar-Terr. Phys., 63, 155–169, 2001.

Hocking, W. K.: Middle Atmosphere dynamical studies at Resolute Bay over a full representative year: planetary waves, tides and special oscillations, Radio Sci., 36, 1795–1822, 2001.

Liu, H.-L., Hagan, M. E., and Roble, R. G.: Local mean state changes due to gravity wave breaking modulated by the diurnal tide, J. Geophys. Res., 105, 12 381–12 396, 2000.

Liu, H.-L. and Hagan, M. E.: Local heating/cooling of the mesosphere due to gravity wave and tidal coupling, Geophys. Res. Letts., 25, 2941–2944, 1998.

Sivjee, G. G. and Walterscheid, R. L.: Six-hour Zonally Symmetric Tidal Oscillations of the winter Mesopause Over the South Pole Station, Planet. Space Sci., 42, 447–453, 1994.

States, R. J. and Gardner, C. S.: Thermal structure of the mesopause region (80–105 km) at 40 K latitude. Part I: Seasonal variations, J. Atmos. Sci., Vol. 57, 66–77, 2000a.

States, R. J. and Gardner, C. S.: Thermal structure of the mesopause region (80–105 km) at 40 K latitude. Part II: Diurnal variations, J. Atmos. Sci., 57, 78–92, 2000b.

Thayaparan, T. and Hocking, W. K.: A long-term comparison of winds and tides measured at London, Canada (43° N, 81° W) by co-located MF and meteor radars during 1994–1999, J. Atmos. Solar Terr. Phys., in press, 2002.

Walterscheid, R. L.: Inertio-gravity wave induced accelerations of the mean flow having an imposed periodic component: Implications for tidal observations in the meteor region, J. Geophys. Res., 86, 9698–9706, 1981.

Walterscheid, R. L. and Hocking, W. K.: Stokes diffusion by atmospheric internal gravity waves, J. Atmos. Sci., 48, 2213–2230, 1991.

Walterscheid, R. L., Sivjee, G. G., Schubert, G., and Hamwey, R. M.: Large Amplitude Semi-Diurnal Variations in the Polar Mesopause: Evidence of a Pseudotide, Nature, 324, 347–349, 1986.

Walterscheid, R. L. and Sivjee, G. G.: Very High Frequency Tides Observed in the Airglow over Eureka (80° N), Geophys. Res. Lett., 23, 3651–3654, 1996.

Walterscheid, R. L. and Sivjee, G. G.: Zonally Symmetric Oscillations Observed in the Airglow from South Pole Station, J. Geophys. Res., 106, 3645–3654, 2001.